# Behavior of Steel Moment Frames using Top-and-Seat Angle Connections under Various Column Removal Scenarios

Kai Qian[1] Ph.D, M.ASCE, Xi Lan[2], Zhi Li[3] and Feng Fu[4], C.Eng, F.ASCE

## ABSTRACT

Top-and-seat angle connection is a conventional type of steel moment connection. However, its capacity in accommodating columns loss is rarely studied. In this study, five multi-story steel moment sub-frames using top-and-seat angle connection were fabricated and tested to investigate their performance subjected to various column removal scenarios including: (a) a middle column loss; (b) a penultimate column loss; and (c) a corner column loss. Moreover, the effects of the thickness of steel angle on load resistance were quantified. The test results indicated that load resisting capacity increased significantly with the increase of angle thickness. In both middle column and penultimate column removal scenarios, catenary action was developed in the frames. It is also noticed that, flexural action dominated the load resisting mechanism of the frames under a corner column loss scenario. For beams in different stories, similar flexural resistance was developed. However, the beams in the first story are able to develop larger catenary action than that in the second story. It worth noting that, for a corner column missing scenario, Vierendeel action helps to enhance the flexural action significantly.

**CE Database subject heading:** experimental; analytical; progressive collapse; steel; moment frame

---

[1] Professor in College of Civil Engineering and Architecture at Guilin University of Technology, China, 541004, (corresponding author) qiankai@glut.edu.cn

[2] Research Student in College of Civil Engineering and Architecture at Guangxi University, China, 530004, lanx@st.gxu.edu.cn

[3] Research Fellow in College of Civil Engineering and Architecture at Guilin University of Technology, China, 531004, lizhi@st.gxu.edu.cn

[4] Senior Lecturer in Structural Engineering, School of Mathematics, Computer Science and Engineering, City, University of London, U.K., Feng.Fu.1@city.ac.uk

## INTRODUCTION

Progressive collapse is defined as the initial local failure leading to the disproportionate collapse of the building. Although progressive collapse is a relatively low likelihood event, considerable loss of live and properties were involved. Thus, deep understanding on its capacity to prevent progressive collapse is essential. After the collapse of Ronan Point building, the alternative load path (ALP) method was proposed as a main direct design method in design guidelines (DoD 2010 and GSA 2013) due to its event independent merit.

In the past decade, relied on ALP method, extensive quasi-static tests were conducted to evaluate the mechanism of steel frames to resist progressive collapse (Lee et al. 2010; Dinu et al. 2016; Qin et al. 2016; Dinu et al. 2017; Tang et al. 2019; Wang et al. 2019; Gao et al. 2017; Qian et al. 2020a). For welded connection, the fracture generally occurred at the beam flanges near the welds (Li et al. 2007; Li et al. 2017). The brittle fracture of weld leads to low deformation capacity, which is essential to the development of catenary action (Li et al. 2018; Qian et al. 2020a). For seismically configured steel frames, to increase the deformation capacity and ductility, reduced beam section (RBS) was adopted for welded connection (Khandelwal and Ei-Tawil 2007; Sadek et al. 2011; Lew et al. 2013; Wang et al. 2020). It was found that flexural action and catenary action were the primary load resisting mechanisms for steel frames subjected to a middle column loss scenario (Alashker et al. 2011; Liu et al. 2015; Meng et al. 2019; Zhong et al. 2020; Dimopoulos et al. 2020; Wang et al. 2016). Compressive arch action was normally ignored in steel frames to resist progressive collapse due to relatively large span-to-depth ratio. However, Lu et al. (2019) found that for composite frames, compressive arch action was developed in steel beams, but the local buckling occurred on the compressive flange at beam end, may reduce the efficiency of compressive arch action.

Compared to welded connections, the bolted angle connection, such as top-and-seat angle connections, exhibits greater ductility and deformation capacity. The seismic behavior of top-and-seat angle connections has been studied extensively (Shen and Astaneh-Asl 1999; Garlock et al. 2003; Danesh et al. 2007; Gong 2014; Abdalla et al. 2015; Davaran et al. 2019; Beland et al. 2020a, b, c). It was found that the angle thickness is one of the most critical parameters on the nonlinear behavior of the connection (Azizinamini 1982; Garlock et al. 2003; Shen and Astaneh-Asl 1999; Abdalla et al. 2015). For connections with thin angles, plastic hinges were formed in the extruded leg of the angles. However, for relatively thick angles, the plastic hinge might form at the central line of the column bolts (Shen and Astaneh-Asl 1999). In addition, based on the deflection shape, a three-linear moment–rotation behavior was proposed by Shen and Astaneh-Asl (1999). Compared to seismic behavior of top-and-seat angle connection, investigations on their progressive collapse behavior are fewer (Yang and Tan 2013a, b; Oosterhof and Driver 2015; Weigand and Berman 2016; and Gong 2017). Yang and Tan (2013a, b) studied different types of steel frames with bolted angle connections under a middle column removal scenario. The behavior and failure modes of different connections are presented and discussed. Gong (2017) found that steel frames with top-and-seat angle connection developed both flexural action and compressive arch action in their tests. A compressive spring model was proposed for simulating progressive collapse behavior of the top-and-seat angle connection.

However, as proposed by DoD (2010) and previous studies (Stevens et al. 2011; Fu 2009,2010,2012), the building should be evaluated extensively under different column missing scenarios including: a) the loss of an interior column, b) the loss of a penultimate column, and c) the loss of a corner column, etc. This is because the development of load resisting mechanism depends on the position of column removal. Different boundary condition should be applied on the tested specimens in accordance with different column removal scenarios. Moreover, studies on steel frames subjected to the loss of a penultimate column or a corner column was rare. Furthermore, although progressive collapse behavior of a structure is a global response, majority of existing tests on steel frames against progressive collapse only relied on simplified single-story beam-column sub-assemblages, ignoring the interaction of structural components in different stories.

Therefore, in this study, five two-story by two-bay 1/2-scale steel sub-frames were fabricated and tested to investigate the load resisting mechanism of the steel frame using top-and-seat angle connections under different column missing scenarios. To deeply understand the load resisting mechanism of steel frames using this type of connections, analytical analysis was also made.

## EXPERIMENTAL PROGRAM

### Test specimens

As shown in Fig. 1, a six-story, 6×6 bay prototype steel moment frame with non-seismic design configuration was fabricated in accordance with AISC-360 (2005). The designed dead and live loads are 5.1 kN/m$^2$ and 3.0 kN/m$^2$, respectively. The story height of the prototype frame is 3.0 m with span length of the frame in longitudinal and transverse direction was 8.4 m by 6.0 m, respectively. Considering fabrication cost and facility capacity of the laboratory, only two-bay by two-story sub-frame was extracted from the prototype frame and scaled down by a factor of 2.0. To simulate horizontal restraints from the surrounding bays, beam was extended with length of 655 mm beyond the side column, if any, as shown in Fig. 2a. As pointed out below, a horizontal roller was utilized to connect the overhanging beam and A-frame.

The geometric details of top-and-seat angle connection are shown in Fig. 3. Although 1/2-scale specimens were tested, the connection configurations, which were scaled down proportionally, were still commonly used as in practice. Chinese section HN 200×100×5.5×8 (equivalent to American W shape of W8×5$^{1/4}$×18 unit in in.) was used for beams whereas HW 150×150×7×10 (equivalent to American W shape of W6×6×20 unit in in.) was for columns. Continuity plates with thickness of 10 mm were provided in the column. Steel angles with size of 70 mm×6 mm, 70 mm ×8 mm, and 70 mm×10 mm was used as top-and-seat angle to connect beam and column flanges. Grade 8.8 M18 bolt were used with nut and washer. Bolts were preload of 345 N·m, which was applied by a torque wrench, was adopted to bolt fastening. Specimen properties are listed in Table 1, in which TSC, TSP, and TSM represent the specimens under a corner, a penultimate, and a middle column removal scenario, respectively. It should be noted that the number 6, 8, and10 represent the thickness of steel angle. For example, TSP-8 represents steel sub-frame with top-and-seated angle connection, which was fabricated by 8 mm thick steel angle, subjected to the loss of a penultimate column scenario.

### Material properties

Chinese Q235 steel was used for column, beam, and angle. The measured yield strength, ultimate strength, and elongation of the angle and structural components are tabulated in Table 2. As no independent coupon test was conducted for bolts (Grade 8.8 M18), the yield stress and ultimate strength of the bolts are the value provided by supplier.

**Test setup**

For TSM-8 and TSP-8, as shown in Figs. 4a and b, the bottom of each edge column was pin supported. The beam overhang, if any, was connected to the A-frame via a roller connection. The columns at ground story were removed at different location prior to applying concentrated load to replicate initial local damage. The vertical load was applied by a hydraulic jack (Item 1 in Fig. 4a) at the top of joints, where a column was removed in advance, by displacement-controlled loading method. This method was relied on the merit of alternate load path method and had been adopted by extensive previous studies (Lee et al. 2010; Sadek et al. 2013, Yang and Tan 2013a, b; Wang et al. 2017; Qian et al. 2020a, b). However, it should be noted that the uniformly distributed live load and dead load were ignored herein, which may change the failure mode and deformation capacity of the specimens (Qian et al. 2020c). To prevent any undesired out-of-plane failure, a steel assembly (Item 3 in Fig. 4a) was installed beneath the hydraulic jack (Item 1 in Fig. 4a). Side column was applied axial force with axial compressive ratio of 0.3 via a hydraulic jack (Item 4 in Fig. 4a) to represent the loads from above floor.

Fig. 4c shows the test setup of TSC-8, which replicated the loss of a corner column. To allow possible rotation of the corner column, a one-way hinge (Item 8 in Fig. 4c) was installed at the top of the corner column. To prevent out-of-plane failure of the beams in ground story, a pair of supporting beams (Item 9 in Fig. 4c) with rollers was installed. As shown in Fig. 2, the strain at critical sections was monitored by a series of strain gauges or strain gauge rosettes. Thus, the axial forces and bending moments of the beam sections could be determined by simplified section analysis.

**Instrumentations**

Instrumentations are shown in Fig. 4. A load cell (Item 2 in Fig. 4a) was installed below the hydraulic jack (Item 1 in Fig. 4a) to measure the applied concentrated load. Tension/compression load cell (Item 5 in Fig. 4a) was installed at each roller to measure its horizontal reaction force. A load pin (Item 6 in Fig. 4a) was installed at each pin support to measure the horizontal reaction force of the bottom pin support. In addition, a series of linear variable differential transformers (LVDTs) (Item 7 in Fig. 4a) were installed along the beam span in ground story, as shown in Fig. 4a.

## EXPERIMENTAL RESULTS

### Vertical load and failure modes

**TSC-8:** The key results are listed in Table 3. The measured load-displacement curves at the joints of the lost column of TSC-8, TSP-8, and TSM-8 are compared in Fig. 5. For TSC-8, the yield load (YL) of 5.1 kN was measured when the displacement at lost column (DLC) reached 40 mm. Therefore, the initial stiffness, which is defined as the ratio of yield load to corresponding yield displacement, of TSC-8 was 0.13 kN/mm. TSC-8 reached the peak load (PL) of 16.6 kN at a DLC of 310 mm. At this displacement stage, fracture occurred at a bottom angle close to the corner column in the second story. Further increasing the displacement, the load resistance started to drop gradually. At a DLC of 345 mm, the bottom angle near the corner column in the second story fractured completely. Then, the top angle close to the corner column in the second story, which was initially suffered compressive force, become in tension. When DLC reached 403 mm, the top angle near the side column in the ground story fractured. However, the load resistance did not loss completely due to the unfractured bottom angle. Further increasing the DLC, the bolted holes of the bottom angle at the corner joint in the first ground were tore off. The bolted holes at the position of column leg of the top angle at the side column in the second story deformed from circular to elliptical, which resulted in the loss of load resistance significantly. The failure mode of TSC-8 is shown in Fig. 6. As shown in the figure, fracture was observed at the bottom angle in Joint A and top angle in Joint B. Although no angle fracture was observed in Joints C and D, the damage was concentrated in the bolted holes, either achieved significant plastic deformation or tearing failure.

**TSP-8**: As shown in Fig. 5, the YL of 11.0 kN was measured at a DLC of 20 mm. Thus, the initial stiffness was 0.55 kN/mm. The right and left bottom angle near the middle column in the ground story fractured at a DLC of 302 mm and 324 mm, respectively. However, after sudden drop of the load resistance due to the angle fracture, the load resistance kept increasing. When the DLC reached 500 mm, the increase of load resistance become gently as the top angle near the side column was yielded at the center-line of the bolts. When the DLC reached 564 mm, the PL of 39.8 kN was recorded. After that, the fracture of angle near the middle column in the second story occurred. The failure mode of TSP-8 is shown in Fig. 7. As shown in the figure, the heel of bottom angle near the middle column fractured at Joints A and B. However, as shown in Joints C and D, although fracture was also occurred at the top angle close to the side column, the fracture of the angle occurred at the center-line of the bolts, which actually performed more ductile.

**TSM-8**：For TSM-8, the YL of 13.5 kN was measured at a DLC of 20 mm. The initial stiffness of TSM-8 is 0.68 kN/mm, which is about 523.0 % and 123.6 % of that of TSC-8 and TSP-8, respectively. The left and right angle near the middle column in the ground story fractured at the DLC of 291 mm and 316 mm, respectively. Compared to TSP-8, the angle fractured earlier. The PL of 44.4 kN, which is 111.7 % of that of TSP-8, is measured at a DLC of 394 mm. At this stage, the bottom angle at the left side of the middle column in the second story fractured. Then, the load resistance dropped over 43.3 % due to the fracture of the bottom angle near the right side of middle column in the second story. Further increasing DLC to 447 mm, 459 mm, and 487 mm, top angles near the side columns were fractured in sequence. However, as shown in Fig. 8, if uniformly distributed dead load and live load was simulated in the test setup, the failure may first occur at the beam end near the side column due to slightly greater bending moment occurred there. Thus, ignoring the uniform distributed live load and dead load may change the failure mode. The failure mode of TSM-8 is shown in Fig. 9. In general, the failure mode of TSM-8 is similar to that of TSP-8.

**TSM-6**：Compared to TSM-8, angle thickness of TSM-6 decreased to 6 mm. As shown in Fig. 10, the YL of 9.3 kN, which is about 68.9 % of that of TSM-8, is measured at a DLC of 19 mm. The PL of 34.0 kN was measured at a DLC of 289 mm. At this displacement stage, the bottom angle near the right side of the middle column fractured. Different to TSM-8, the load resistance of TSM-6 kept decreasing after the angle fracture first occurred due to the remaining angles fractured soon. Similar to TSM-8, the fracture of the angle in the second story was later than that in the ground story. Moreover, the fracture of the angle near the middle column was occurred earlier than that near the side column. The failure mode of TSM-6 is shown in Fig. 11.

**TSM-10**：Compared to TSM-8, thicker angle of 10 mm was used in TSM-10. The YL of 21.4 kN, which is about 158.5 % and 230.1 % of that of TSM-8 and TSM-6, is measured at a DLC of 23 mm. The greater YL measured in TSM-10 is mainly because that the first yield was measured at the beam flange, rather than at the angle. Different to TSM-8 and TSM-6, the load resistance kept increasing until the DLC reached 425 mm due to tear failure of the beam flange near the middle column in the ground story. The PL of TSM-10 is 106.2 kN, which is 239.2 % and 312.4 % of that of TSM-8 and TSM-6, respectively. Further increasing DLC to 483 mm, the top angle near the side column in the second story fractured. After that, the fracture of angle occurred in sequence. The failure mode of TSM-10 was presented in Fig. 12. Different to TSM-8 and TSM-6, tear failure of the beam flanges near the middle column in the ground story was observed.

**Horizontal reaction force**

Fig. 13 shows the horizontal reaction force (negative and positive values represent compressive and tensile reaction force, respectively.) From the figure, initial compressive reaction force was measured in TSP and TSM specimens. Thus, compressive arch action actually was developed in the beams either subjected to a penultimate column or interior column scenario. The maximum compressive reaction force in TSP-8, TSM-8, TSM-6, and TSM-10 was -12.4 kN, -13.4 kN, -12.1 kN, and -16.1 kN, respectively. Therefore, even without overhanging beams, TSP-8 developped similar compressive arch action as that of TSM-8. Increasing the thickness of steel angle will not enhance compressive arch action significantly. However, for TSM-10, as the first yield was occurred at the beam flange rather than the steel angle, larger yield load and compressive arch action developed. As the compressive reaction force is relatively low, the compressive arch action is insignificant, which agrees with the findings from previous studies (Yang and Tan 2013a, b). As the span/depth ratio in steel beams are much larger than that of reinforced concrete beams, compressive arch action for tested specimens is insignificant. Therefore, in later discussion, the compressive arch action was included in flexural action. Moreover, for all specimens, majority of compressive reaction force was attributed to the bottom pin support except for TSM-6, which was mainly attributed to the second story. In large deformation stage, tensile reaction force was measured including TSP-8. The maximum tensile reaction force of TSP-8, TSM-8, TSM-6, and TSM-10 was 27.0 kN, 82.7 kN, 57.9 kN, and 179.7 kN, respectively. Thus, contrary to compressive arch action, without overhanging beams in TSP-8 resulted in much lower tensile reaction force and catenary action. Moreover, increasing the thickness of the steel angle could increase catenary action significantly. For TSM-10, much greater catenary action was developed mainly due to the thicker angle changed the failure mode of the specimen (fracture of the beam flange, rather than fracture of the steel angle). Different to compressive reaction force, the tensile reaction force was almost provided by the bottom pin support and second story equally.

**Deformation measurements**

As shown in Fig. 14, outward movements were observed initially through horizontally installed LVDTs. Compared to the joints without overhanging beams, the joints with overhanging beams showed lower outward movements (refer to Fig. 14a). Moreover, the joint in the second story achieved greater outward movements than that in the first story. Similarly, greater inward movements were measured in the joints without overhanging beams. Compared to TSP-8, TSM-8 measured much lower outward movements, as shown in Fig. 14b. However, the inward movements of TSM-8 actually were greater than that of the joints with overhanging beams in TSP-8. This is mainly due to greater tensile force developed in TSM-8, which pulled the steel angle to achieve greater horizontal deformation. As shown in Figs. 14b-d, TSM-8, TSM-6, and TSM-10 achieved similar inward movements in the joints. This could be explained that although TSM-10 developed the largest tensile force, the steel angle in TSM-10 has largest horizontal stiffness. Similarly, the tensile force in TSM-6 is least. However, 6 mm thickness angle in TSM-6 resulted in the lowest horizontal stiffness. Therefore, the maximum inward movement of TSM-6, TSM-8, and TSM-10 is similar.

Fig. 15 shows the deflection shape of the beams with various stages. As shown in Fig. 15a, for TSC-8, the deformation shape of the beam in corner bay close to the deformation of a cantilever beam under a concentrated load. The chord rotation, which is defined as the ratio of DLC to beam span, will overestimate the rotation of the beam near the interior column but under-estimate the rotation of the beam end near the lost corner column. However, different to TSC-8, as shown in Fig. 15b, double curvature deformation shape was observed in TSM-8. Conversely, the chord rotation could accurately estimate the rotation of the beam near the side column but over-estimate the rotation of the beam near the middle column. Furthermore, the deformation was concentrated at the angles rather than the beams. Similar phenomenon was found in previous studies (Hasan et al. 2017; Kong and Kim 2017). For TSP-8, TSM-6, and TSM-10, similar results were observed.

**Internal force measurements**

To further understand the load resisting mechanism, the internal forces, such as axial force and bending moment in beams, should be quantified from the test results. The reliability of strain gauge results to determine the load resistance of tested specimens was first evaluated. The calculation method has been described in detail in authors' previous work (Qian et al. 2020a). As shown in Fig. 2b, strain gauges installed in Sections A1-4 or A1-8 were utilized for bending moment calculation while strain gauges installed in Sections B1-4 or B1-8 were utilized for determination of the axial force. Figs. 16 and 17 compare the vertical load-displacement curves and horizontal reaction force-displacement curves based on the results of load cell and strain gauges, respectively. From the figures, it was found that, generally, the analytical results from strain gauge readings agree with the measured value from load cells well, except at the location of fracture in either steel angle or beam flanges. Therefore, the strain gauge results are reliable to be used in further discussion.

Based on strain gauge results, Fig. 18 illustrates the de-composition of load resistance from different load resisting mechanisms. As shown in Fig. 18a, for TSC-8, the load resistance purely relied on flexural action during test. For TSP-8, as shown in Fig. 18b, considerable catenary action was developed even one side column did not have overhanging beams (no horizontal constraints from surrounding bays). The maximum contribution of catenary action is 48.1 % for TSP-8. However, before fracture of the steel angle, majority of the load resistance was also attributed into flexural action.

For TSM-series specimens, similar to TSP-8, catenary action was kicked-in in large deformation stage. Compared to TSP-8, the contribution of catenary action in large deformation stage was much greater. The maximum contribution of catenary action of TSM-8, TSM-6, and TSM-10 was 358.4 %, 95.6 %, and 124.6 %, respectively. The contribution of catenary action was even larger than the total load resistance, which could be explained by the contribution of flexural action was negative in large deformation stage, which can be explained as the compressive angle become tensile angle after the original tensile angle was fractured.

## DISCUSSION OF TEST RESULTS

### Load resistance capacity at different stories

Unlike previous studies (Sadek et al. 2011; Yang and Tan 2013a; Wang et al. 2016; Zhong et al. 2020), two-story sub-frames was fabricated and tested in this study to evaluate the difference of the development of load resisting mechanisms in different stories. Thus, based on the strain gauge results, the contribution of load resistance from different stories was determined and presented in Fig. 19. As shown in Figs. 19a and b, for TSC-8 and TSP-8, before failure first occurred at the connection, the load resistance from the first and second story is similar. For TSM-8, TSM-6, and TSM-10, as shown in Figs. 19c, d, and e, the load resistance from the first and second story is similar at early stage of the test. However, when the DLC reached 90 mm, 125 mm, and 150 mm, the load resistance of first story exceeded that of second story for TSM-8, TSM-6, and TSM-10, respectively. To reveal the difference further, the flexural action and catenary action of each story were calculated and shown in Fig. 20. As shown in Fig. 20, the flexural action developed in the first and second story is similar prior to first fracture of the angle or beam flange. However, the catenary action developed in the first story is always greater than that in the second story. Thus, for TSC-8 and TSP-8, the load resistance from the first and second story is similar as flexural action dominated the load resistance. However, for TSM-series specimens, catenary action dominated the load resistance in large deformation stage, resulting in greater load resistance from the first story in large deformation stage.

**Effects of the position of column removal**

Fig. 5 compares the vertical load response under various column removal scenarios. The initial stiffness of TSM-8 and TSP-8 was much larger than that of TSC-8. The initial stiffness of TSC-8, TSP-8, and TSM-8 was 0.13, 0.55 and 0.68 kN/mm, respectively. Moreover, the PL of TSC-8, TSP-8, and TSM-8 was 16.6 kN, 39.8 kN, and 44.4 kN, respectively. Thus, the initial stiffness of TSC-8 was only 18.9 % of that of TSM-8. This was because the beams of TSC-8 worked as cantilever beam in flexural action stage, while plastic hinge was formed in two beam ends in TSM-8. Thus, for TSC-8, the number of plastic hinges was only 1/4 of that of TSM-8. However, the PL of TSC-8 was 37.4 % of that of TSM-8. This indicated that partial plastic hinges were formed at the beam end near the corner connection of TSC-8 due to Vierendeel action. Therefore, for a moment resisting frame, the Vierendeel action should be considered to evaluate the load resisting capacity of the frames subjected to the loss of a corner column scenario. However, majority of existing tests (Stylianidis et al. 2016b; Hou et al. 2016; Wang et al. 2017) conservatively treated the beam as a cantilever beam in corner column removal scenario. This is because these tests based on single-story beam-column sub-assemblages, it is unable to replicate the interaction between the structural components in different stories (merit of Vierendeel action) well. The initial stiffness and PL of TSP-8 is 80.9 % and 89.6 % of that of TSM-8. It indicated that the lack of horizontal constraints would slightly decrease the load resistance of the specimen. The vertical displacement corresponding PL of TSC-8, TSP-8, and TSM-8 was 310 mm, 564 mm, and 394 mm, respectively. Thus, the vertical displacement corresponding PL of TSC-8 was only 78.7% of that of TSM-8. However, the vertical displacement corresponding PL of TSP-8 was 143.1% of that of TSM-8 due to the side column without horizontal constraints were able to move inwards to the middle column in the large deformation stage, which would effectively delay the fracture of steel angle. Analyzing the results, the loss of a corner column is the most critical scenario among all the cases. As shown in Fig. 18a, the absence of adequate horizontal constraints in the case of corner column removal, resulting in limited catenary action developed, which is the second line of defense.

### 4.3. Effects of angle thickness

Fig. 10 illustrates the effects of angle thickness on the performance of steel frames. The initial stiffness of TSM-6, TSM-8, and TSM-10 was 0.49, 0.68 and 1.12 kN/mm, respectively. Compared to TSM-8, the initial stiffness of TSM-6 decreased by 27.9 % while TSM-10 increased by 64.7 %. In addition, the PL of TSM-6, TSM-8, and TSM-10 was 34.0 kN, 44.4 kN, and 106.2 kN, respectively. The increasing the angle thickness from 6 mm to 8 mm, the PL only increased by 30.6 %. However, increasing the angle thickness from 8 mm to 10 mm, the PL could increase by 139.2 %. This is because, compared to TSM-8, TSM-10 was failed at the beam flange, rather than at the steel angle. Furthermore, the DLC corresponding PL of TSM-6, TSM-8, and TSM-10 was 289 mm, 394 mm, and 425 mm, respectively. Thus, increasing the angle thickness, the deformation capacity of the steel frame was also increased. It should be emphasized that different from TSM-6 and TSM-8, which were fractured at the heel of the angle, for TSM-10, the plastic hinges were formed along the bolt center-lines, which increased the deformation capacity (Yang and Tan 2012; Pirmoz et al. 2009).

## ANALYTICAL ANALYSIS

Although experimental tests were performed to investigate the influences of different column missing scenarios and angle thickness, as the number of tested specimens is relatively few, an analytical model was developed here to further understand the capacity of steel frames with top-and-seat angle connections to resist progressive collapse.

### Middle column removal

Based on analysis of the test results, the load resistance of steel frames could be calculated by summation of the load resistance from flexural action and catenary action, as expressed by Eq. 1. Considering the difference between different stories, in this analytical model, it was assumed similar flexural action developed in different stories while the discrepancy on catenary action was considered.

$$P^{middle} = P_{FA} + P_{CA} \tag{1}$$

#### *Flexural action*

For flexural action resistance, a bilinear moment-rotation model was adopted by assuming force-deformation characteristics at both sides of connections was identical, as shown in Fig. 21.

According to (Bruneau et al. 1997), the yield moment of an angle leg section is 0.667 times its plastic moment. The connection yield moment can be expressed by Eq. 2:

$$M_y = M_p / 1.5 \tag{2}$$

An equation from Pirmoz et al. (2009) is used to evaluate the plastic moment of the connection:

$$M_p = \frac{\beta M_{p-angle}}{g} h_b \tag{3}$$

where $\beta$ is the parameter used to accurately estimate the effect of variates that affect the pattern of mechanism which can be found in Pirmoz et al. (2009), $M_{p-angle}$ is the plastic moment capacity of the tensile angle leg which can be calculated by Eq. 4; $g$ is the gage distance of the tensile angle as shown in Fig. 22a, $h_b$ is the beam depth.

The plastic moment capacity of the tensile angle with material strength $f_y$, width $b$, and thickness $t$, can be determined as follow:

$$M_{p-angle} = \frac{f_y b t^2}{4} \tag{4}$$

As suggested by Pirmoz et al. (2009), the initial stiffness $K_i$ and the tangent stiffness of the connection $K_{py}$ can be calculated by Eqs. 5-7.

$$K_i = h_b^2 K_{ta} \tag{5}$$

$$K_{ta} = \frac{1}{\frac{1}{\alpha K_1} + \frac{1}{K_3}} \tag{6}$$

$$K_{py} = \left(c\alpha - d\right) K_i \tag{7}$$

In above equations, $K_{ta}$ is the equivalent stiffness of the springs of the tensile angle vertical leg ($K_1$), the bolt axial stiffness ($K_2$), and the bolt flexural stiffness ($K_3$) in series, as shown in Fig. 22b. Ignoring axial deformation of the column bolts, $K_{top}$ can be calculated by Eq. 6. $\alpha$ is a modification factor for the flexural stiffness; $c$ and $d$ are the parameters to consider the effects of different material properties. The equations for determination of $K_1$, $K_3$, $\alpha$, $c$, and $d$ can be found from Pirmoz et al. (2009) in detail.

Before the connection yielding, the load resistance of the frame was only provided by flexural action. For the specimens under middle column removal scenario, the yield displacement $u_y^{middle}$ and yield load $P_y^{middle}$ were determined by Eqs. 8 and 9, respectively.

$$u_y^{middle} = M_y L / K_i \tag{8}$$

$$P_y^{middle} = 2 \times 2 \times \frac{2M_y}{L} \tag{9}$$

where $L$ is the span length.

In post yield stage, the relationship between vertical displacement $u$ and flexural action as shown in below:

$$M_{py} = M_y + \frac{K_{py}\left(u - u_y^{middle}\right)}{L} \tag{10}$$

$$P_{FA}^{middle} = 2 \times 2 \times \frac{2M_{py}}{L} \tag{11}$$

***Catenary action***

Assuming the column with sufficient horizontal constraints have full connectivity with the angle, the axial deformation of the beams can be determined based on the second-order approximation and expressed as Eq. 12 (Stylianidis et al. 2016a), as shown in Fig. 23a. It should be noted that the axial deformation of the beam is twice the deformation of a single angle connection as a beam has two angle connection.

$$\Delta = \Delta^b/2 = L(1-\cos\theta)/2 = u^2/(4L) \tag{12}$$

It should be noted that catenary action began to develop once the axial deformation exceeded the gap in the angle connection. As the designed allowance of bolts was 1 mm, the gap related to axial deformation ( $\Delta_{gap}^{1st}$ ) is 2 mm for the beams in the first story. As the gaps in the first story will affect the formation of catenary action in the second story, the gap ( $\Delta_{gap}^{2nd}$ ) is 4 mm for the beams in the second story.  The behavior of spring load-deformation relationship is shown in Fig. 23b. Based on the force equilibrium, the catenary action of each story can be calculated according to Eq. 13.

$$P_{CA} = \frac{K_s\left(u - u_{\Delta gap}\right)^3}{L^2} \tag{13}$$

where $K_s$ is the spring stiffness, which will be introduced in detail as following; $u_{\Delta gap}$ is the vertical displacement in accordance with $\Delta_{gap}$ ($u_{\Delta gap} = \sqrt{4L\Delta_{gap}}$ based on Eq. 12).

For TSM-6 and TSM-8, the failure mode was controlled by angle fracture. The elastic stiffness of the spring in the ground story $K_s^{1st}$ , as proposed by Faella et al. (2000), can be determined as Eq. 14.

$$K_s^{1st} = K_{at} = \frac{0.5 b_{eff} t^3 E}{m^3}\left(\frac{4\gamma}{4\gamma + 3}\right) \tag{14}$$

where $b_{eff}$ is the effective width of the angle which can be obtained in Faella et al. (2000), $E$ is the Young's modulus, the geometric parameter $m$ and the coefficient $\gamma = \frac{I_2/L_2}{I_1/L_1}$ are shown in Fig. 24.

Based on experimental results, the elastic stiffness of the spring in the second story ( $K_s^{2nd}$ ) is about 0.4 of that of $K_s^{1st}$ . It was assumed that the specimen reached its ultimate capacity when the axial force of ground story $N^{1st} = P_{CA}^{1st} / \sin\theta$ exceeds the bending resistance of the tensile angle ($F_{T,Rd}$), as shown in Eq. 15.

$$F_{T,Rd} = \frac{4M_{y,Rd}}{m} = \frac{b_{eff} t^2 f_y}{m} \quad (15)$$

For TSM-10, as fracture occurred at the beam flange, rather than at a steel angle. The spring stiffness $K_s'$ (to distinguish $K_s$ is Eq. 13) should be determined as Eq. 16, where the stiffness of angle in tension ($K_{at}$), the stiffness of beam flange in bearing ($K_{fb}$), and the stiffness of angle in bearing ($K_{ab}$) are equivalently considered.

$$K_s' = \frac{1}{\frac{1}{K_{at}} + \frac{1}{K_{fb}} + \frac{1}{K_{ab}}} \quad (16)$$

where $K_{at}$ could be determined by Eq. 14, $K_{fb}$ and $K_{ab}$ could be determined by Eq. 17, as suggested by Rex et al. (2003). It should be noted that Eq. 17 is proposed for bearing stiffness of a single plate with a single bolt. For tested angle, two bolts were utilized. Thus, $K_b$ should be $2K_b'$ herein. Moreover, for $K_{fb}$ and $K_{ab}$, the geometric and material properties of beam flange and angle were utilized, respectively.

$$2K_b' = 2\left(\frac{1}{\frac{1}{K_{br}} + \frac{1}{K_b} + \frac{1}{K_v}}\right) \quad (17)$$

The bearing stiffness $K_{br} = 120 t_p f_{yp} \left(d_b / 25.4\right)^{0.8}$, bending stiffness $K_b = 32 E_p t_p \left(L_e / d_b - 0.5\right)^3$ and shear stiffness $K_v = 6.67 \mathrm{G}_p t_p \left(L_e / d_b - 0.5\right)$; in which $G_p$ is the shear modulus of the steel plate, $L_e$ is the distance from bolt center to plate edge.

For TSM-10, it was assumed that failure occurred when the beam axial force exceeded the bearing capacity of the beam flange, as shown in Eq. 18 (Liu et al. 2015).

$$F_{fb,Rd} = \min\left(L_e, 2.76d_b\right) \times f_{uf} t_f \quad (18)$$

**Penultimate column removal**

The stiffness of horizontal constraints of the steel frame subjected to the loss of a penultimate column scenario was determined by the side column without overhanging beams. Thus, it was not accurate to assume similar horizontal constraints to that from the side column with overhanging beams. For simplicity, a reduction coefficient of $\lambda$=0.75 is assumed to related to the case of loss middle column scenario. Similar to the case of loss of a middle column, it was assumed that the specimen failure when the axial force of ground story $N^{1st} = P_{CA}^{1st} / \sin\theta$ exceeds the bending resistance of tensile angle ( $F_{T,Rd}$ ), as shown in Eq. 15. Thus, the load resistance of the frame subject to the loss of a penultimate column was determined by Eq. 19.

$$P^{penultimate} = \lambda P^{middle} \quad (19)$$

**Corner column removal**

Vierendeel action was found to resist progressive collapse in TSC-8. Thus, the corner column in the second story has partial rotational constraints to the beam end. As suggested by Qian and Li (2015), a rotational constraint effectiveness factor $\xi$=0.7 was utilized to evaluate the extent of the rotational constraints in the corner joint. The yield load of TSC-8 is determined in Eq. 20.

$$P_y^{corner} = 2 \times \frac{\left(1+\xi\right) M_y}{L} \quad (20)$$

Qian and Li (2015) indicated that the real boundary condition of the corner column removal scenario (Fig. 25c) lay between the full (Fig. 25a) and free constraints (Fig. 25b). For full rotational constraint mode l ( $\xi$=1), the yield displacement is expressed as below:

$$u_y^{full} = \frac{\phi_y}{6} L^2 \tag{21}$$

where $\phi_y$ is the yield curvature at fixed support in Fig. 25a.

For partial rotational constraint model ($\xi$=0.7), the yield displacement is expressed as below:

$$u_y^{partial} = \frac{\phi_y L^2}{6}\left(2-\xi\right) \tag{22}$$

Thus, yield displacement under corner column removal scenario can be expressed as in Eq. 23.

$$u_y^{corner} = \frac{u_y^{partial}}{u_y^{full}} u_y^{middle} = \left(2-\zeta\right) u_y^{middle} \tag{23}$$

As flexural action is considered in the prediction of TSC-8 and the progressive collapse resistance in post yield stage can be expressed as in Eq. 24.

$$P_{py}^{corner} = 2 \times \frac{\left(1+\xi\right) M_{py}}{L} \tag{24}$$

Similarly, for TSC-8, the vertical displacement corresponding the first fracture can be expressed as in Eq. 25.

$$u_{FF}^{corner} = \left(2-\xi\right) u_{FF}^{middle} \tag{25}$$

where $u_{FF}^{middle} = \sqrt[3]{\dfrac{F_{t,\mathrm{Rd}} L^2 \sin\theta}{K_s}} + u_{\Delta gap}^{1st}$ is the vertical displacement corresponding the first fracture of TSM-8.

**Verification of analytical model**

Fig. 26 compares the analytical load-displacement curve of tested specimens with those from tests. The key results of these curves are tabulated in Table 4. In general, the analytical models predict the initial stiffness, yield load, and first fracture of the steel angle or beam flange well. However, the analytical models could not predict the decreasing of the load resistance after first fracture.

## CONCLUSIONS

In this paper, five two-story steel sub-frames with top-and-seat connections were tested under different column missing scenarios. A series of analytical models were adopted and further developed to predict the load resisting capacity of tested specimens. Based on experimental and analytical results, conclusions are drawn:

1. It was found that the load resisting capacity and deformation capacity of TSC-8 are only 37.4 % and 78.7 % of that of TSM-8. TSP-8 achieved 89.6 % of the load resisting capacity of TSM-8. However, Compared to TSM-8, the deformation capacity of TSP-8 increased by 43.1 %.
2. The load resisting mechanisms of TSP-8 are similar to that of TSM-8, flexural action and catenary action were able to develop to resist progressive collapse. However, catenary action of TSP-8 was commenced much later than TSM-8. For TSC-8, only flexural action is developed during test. Moreover, the partial rotational constraints from the corner column in the second story due to Vierendeel action should be considered for determination of flexural action of the frame under the loss of a corner column scenario.
3. When the angle thickness increased from 6 mm to 8 mm, the load resisting capacity increased by 30.6 %. However, when the angle thickness increased from 8 mm to 10 mm, the load resisting capacity increased by 139.2 %, which is mainly due to the thicker angle changed the failure mode of the frame from angle fracture to the fracture of the beam flange.
4. Test results indicated that, an effective way to improve the performance of steel moment frames against progressive collapse by increasing the angle thickness. Moreover, considering the beneficial of large deformation capacity, which is important for development of catenary action, of the frame with top-and-seat angle connection, the performance of the frames with top-and-seat angle connection against progressive collapse was reliable and should be recommended.
5. The rotational constraint difference between the first and second story has little influence on

the flexural action. Thus, similar load resistance developed in the first and second story before first fracture occurred. However, compared with second story, the larger horizontal constraints for the beams in the ground story resulted in greater catenary action developed in the first story. Multi-story sub-frames were recommended for investigation on behavior of moment frames to resist progressive collapse, especially for the scenario of loss of a corner column.

6. Proposed analytical analysis could reasonably predict the load-displacement curve before the first fracture occurred in the angle or beam flange. However, the models are unable to predict the softening part of the load-displacement curve.


## ACKNOWLEDGEMENTS

This research was supported by a research grant provided by the Natural Science Foundation of China (Nos.52022024, 51778153). Any opinions, findings and conclusions expressed in this paper are those of the writers and do not necessarily reflect the view of Natural Science Foundation of China.


## DATA AVAILABILITY

Some or all data, models, or code that support the findings of this study are available from the corresponding author upon reasonable request.

## FUTURE WORK

As the slab may affect the load redistribution capacity of steel frames with different connections significantly, it was necessary to carry out more tests on three-dimensional multi-story and multi-bay steel substructures including slabs subjected to different column missing scenarios in the future. Additionally, as mentioned in the section of “Test setup”, the commonly used push-down loading method, which is ignored the uniformly distributed dead load and live load, is adopted in this study. This may affect the failure mode and deformation capacity as well as catenary action capacity of the specimens. As no studies had been carried out on steel frames for progressive collapse included or excluded the effects of uniformly distributed loads, it is necessary to do relevant studies in the future.

## REFERENCES

Abdalla, K. M., G. A. Drosopoulos, and G. E. Stavroulakis. (2015). “Failure behavior of a top and seat angle bolted steel connection with double web angles.” J. Struct. Eng. 141 (7): 04014172.

Alashker, Y., and Li, H. H., Ei-Tawil, S. (2011). “Approximations in Progressive Collapse Modeling.” J. Struct. Eng, 137 (9): 914-924.

ANSI (2005). “Specification for Structural Steel Buildings.” ANSI/AISC 360-16. Chicago, Illinois, USA.

Azizinamini, A. (1982). “Monotonic Response of Semi-Rigid Steel Beam to Column Connections.” M.Sc. thesis, College of Engineering, Univ. of South Carolina.

Beland, T., Tremblay, R., Hines, E. M., and Fahnestock L. A. (2020a). “Rotational Capacity of Bolted Double-Web-Angle Beam-Column Gravity Connections through Full-Scale Experimental Testing.” J. Struct. Eng. 146(7): 04020111.

Beland, T., Tremblay, R., Hines, E. M., and Fahnestock L. A. (2020b). “Full-Scale Cyclic Rotation and Shear-Load Testing of Double Web with Top and Seat Angle Beam-Column Connections.” J. Struct. Eng. 146(8): 04020164.

Beland, T., Bradley, C. R., Nelson J., Sizemore J. G., Davaran, A., Tremblay, R., Hines, E. M., and Fahnestock L. A. (2020c). “Experimental Parametric Characterization of Bolted Angle Connection Behavior.” J. Struct. Eng. 146(8): 04020160.

Bruneau, M., Uang, C. M., and Whittaker, A. (1997). “Ductile Design of Steel Structures.” New York (NY): McGraw-Hill: 480.

Davaran, A., Beland, T., and Tremblay, R. (2019). “Elastic-Plastic Analysis of Bolted Angles Usable in Steel Frame Connections.” J. Struct. Eng. 145(7): 04019048.

Danesh, F., A. Pirmoz, and A. S. Daryan. (2007). “Effect of Shear Force on the Initial Stiffness of Top and Seat Angle Connections with Double Web Angles.” J. Constr. Steel Res. 63 (9): 1208–1218.

Dimopoulos, C. A., Freddi. F., Karavasilis, T. L., and Vasdravellis, G., (2020). “Progressive Collapse Resistance of Steel Self-Centering MRFs Including the Effects of the Composite Floor.” Eng. Struct. 206: 110143.

Dinu, F., Marginean, I., and Dubina, D. (2017). “Experimental Testing and Numerical Modelling of Steel Moment-Frame Connections under Column Loss.” Eng. Struct. 150: pp. 861-878.

Dinu, F., Marginean, I., Dubina, D., and Petran, I. (2016). “Experimental Testing and Numerical Analysis of 3D Steel Frame System under Column Loss.” Eng. Struct. 113: 59-70.

DoD (2010). “Design of Building to Resist Progressive Collapse.” UFC 4-023-03. Washington, DC, USA.

Faella, C., Piluso, V., and Rizzano, G. (2000). “Structural Steel Semirigid Connections: Theory, Design and Software.” New directions in civil engineering. Boca Raton (FL (EEUU)). CRC Publishers.

Fu, F. (2009). Progressive collapse analysis of high-rise building with 3-D finite element modeling method. Journal of Constructional Steel Research, 65(6), pp. 1269–1278

Fu, F. (2010). 3-D nonlinear dynamic progressive collapse analysis of multi-storey steel composite frame buildings — Parametric study. Engineering Structures, 32(12), pp. 3974–3980

Fu, F. (2012). “Response of a Multi-Storey Steel Composite Building with Concentric Bracing under Consecutive Column Removal Scenarios.” J. Constr. Steel Res. 70: 115–126.

Gao, S., Guo, L. H., Fu F, and Zhang, S. (2017). “Capacity of Semi-Rigid Composite Joints in Accommodating Column Loss.” J. Constr. Steel Res. 139: 288-301.

Gong, Y. (2014). “Ultimate Tensile Deformation and Strength Capacities of Bolted-Angle Connections.” J. Constr. Steel Res. 100 (6): 50–59.

Gong, Y. (2017). “Test, Modeling and Design of Bolted-Angle Connections subjected to Column Removal.” J. Constr. Steel Res. 139: 315–326.

Garlock, M., J. M. Ricles, and R. Sause. (2003). “Cyclic Load Tests and Analysis of Bolted Top-and-Seat Angle Aonnections.” J. Struct. Eng. 129 (12): 1615–1625.

GSA (2013). “Progressive Collapse Analysis and Design Guidelines for New Federal Office Buildings and Major Modernization Projects.” Washington, DC, USA.

Hasan, M. J., Ashraf, M., and Uy, B. (2017). “Moment-Rotation Behaviour of Top-Seat Angle Bolted Connections Produced from Austenitic Stainless Steel.” J. Constr. Steel Res. 136 (2): 149-161.

Hou, J., Song, L., and Liu, H. H. (2016). “Testing and Analysis on Progressive Collapse-Resistance Behavior of RC Frame Substructures under a Side Column Removal Scenario.” J. Perform. Constr. Facil. 30 (5): 04016022.

Khandelwal, K., and Ei-Tawil, S. (2007). “Collapse Behavior of Steel Special Moment Resisting Frame Connections.” J. Struct. Eng. 133 (5): 646-655.

Kong, Z. Y., and Kim, S. E. (2017). “Numerical Estimation for Initial Stiffness and Ultimate Moment of Top-Seat Angle Connections without Web Angle.” J. Struct. Eng. 143 (10): 04017138.1-04017138.15.

Lee, C. H., Kim, S., and Lee, K. (2010). “Parallel Axial-Flexural Hinge Model for Nonlinear Dynamic Progressive Collapse Analysis of Welded Steel Moment Frames.” J. Struct. Eng. 136 (2): 165-173.

Lew, H. S., Main, J. A., Robert, S. D., Sadek, F., and Chiarito, V. P. (2013). “Performance of Steel Moment Connections under a Column Removal Scenario. I: Experiments.” J. Struct. Eng. 139 (1): 98-107.

Li, H. H., Cai, X. H., Zhang, L., Zhang, B. Y., and Wang, W. (2017). “Progressive Collapse of Steel Moment-Resisting Frame Subjected to Loss of Interior Column: Experimental Tests.” Eng. Struct. 150: 203-220.

Li, L., Wang, W., Chen, Y. Y., and Teh, L. H. (2007). “Column-Wall Failure Mode of Steel Moment Connection with Inner Diaphragm and Catenary Mechanism.” Eng. Struct. 131: 553-563.

Li, L. L., Li, G. Q., Jiang, B. H., and Lu, Y. (2018). “Analysis of Robustness of Steel Frames against Progressive Collapse.” J. Constr. Steel Res. 143: 264–278.

Liu, C., Tan, K. H., and Fung, T. C. (2015). “Component-Based Steel Beam-Column Connections Modelling for Dynamic Progressive Collapse Analysis.” J. Constr. Steel Res. 107: 24-36.

Liu, C., Tan, K. H., and Fung, T. C. (2015). “Investigations of Nonlinear Dynamic Performance of Top-And-Seat with Web Angle Connections Subjected to Sudden Column Removal.” Eng. Struct. 99: 449-461.

Lu, X. Z., Zhang, L., Lin, K. Q., and Li, Y. (2019). “Improvement to Composite Frame Systems for Seismic and Progressive Collapse Resistance.” Eng. Struct. 186: 227-242.

Meng. B., Zhong, W. H., Hao, J. P., Song, X. Y., and Tan, Z. (2019). "Calculation of the Resistance of an Unequal Span Steel Substructure Against Progressive Collapse Based on the Component Method." Eng. Struct. 182: 13-28.

Oosterhof, S. A. and Driver, R. D. (2015). "Behavior of Steel Shear Connections under Column Removal Demands." J. Struct. Eng. 141(4): 04014126.

Weigand, J. M. and Berman, J. W. (2016). "Integrity of Bolted Connections Subjected to Simulated Column Removal." J. Struct. Eng. 142(3): 04015165.

Pirmoz, A., Khoei, A. S., Mohammadrezapour, E., and Daryan, A. S. (2009). "Moment-Rotation Behavior of Bolted Top-Seat Angle Connections." J. Constr. Steel Res. 65 (4): 973-984.

Qian, K., and Li, B. (2015). "Analytical Evaluation of the Vulnerability of RC Frames for Progressive Collapse Caused by the Loss of a Corner Column." J. Perform. Constr. Fac. 29 (1): 04014025.

Qian, K., Lan, X., Li, Z., Li, Y., and Fu, F. (2020a). "Progressive Collapse Resistance of Two-Storey Seismic Configured Steel Sub-Frames Using Welded Connections." J. Constr. Steel Res. 170: 106117.

Qian, K., Liang, S. L., Xiong, X. Y., Fu, F., and Fang, Q. (2020b). "Quasi-Static and Dynamic Behavior of Precast Concrete Frames with High Performance Dry Connections Subjected to Loss of a Penultimate Column Scenario." Eng. Struct. 205: 110115.

Qian, K., Liang, S. L., Feng, D. C., Fu, F., and Wu, G. (2020c). "Experimental and Numerical Investigation on Progressive Collapse Resistance of Post-Tensioned Precast Concrete Beam-Column Subassemblages." J. Struct. Eng., 146(9): 04020170.

Qin, X., Wang, W., Chen, Y. Y., and Bao, Y. H. (2016). "A Special Reinforcing Technique to Improve Resistance of Beam-to-Tubular Column Connections for Progressive Collapse Prevention." Eng. Struct. 2016; 17: 26-39.

Rex, C., and Easterling, W. (2003). "Behaviour and Modelling of a Bolt Bearing on a Single Plate." J. Struct. Eng. 192 (6): 792–801.

Sadek, F., Main, J. A., Lew, H. S., and Bao, Y. H. (2011). "Testing and Analysis of Steel and Concrete Beam-Column Assemblies under a Column Removal Scenario." J. Struct. Eng. 137 (9): 881-892.

Shen, J., and A. Astaneh-Asl. (1999). “Hysteretic Behavior of Bolted-Angle Connections.” J. Constr. Steel Res. 51 (3): 201–218.

Shen, J., and A. Astaneh-Asl. (2000). “Hysteresis Model of Bolted-Angle Connections.” J. Constr. Steel Res. 54 (3): 317–343.

Stevens, D., Crowder, B., Sunshine, D., Marchand, K., Smilowitz, R., Williamson, E., and Waggoner, M. (2011). “DoD Research and Criteria for the Design of Buildings to Resist Progressive Collapse.” J. Struct. Eng. 137 (9): 870-880.

Stylianidis, P. M., Nethercot, D. A., Izzuddin, B. A., and Elghazouli, A. Y. (2016a). “Robustness Assessment of Frame Structures Using Simplified Beam and Grillage Models.” Eng. Struct. 115: 78–95.

Stylianidis, P. M., Nethercot, D. A., Izzuddin, B.A., and Elghazouli, A.Y. (2016b). “Study of the Mechanics of Progressive Collapse with Simplified Beam Models.” Eng. Struct. 117: 287-304.

Tang, H. Y., Deng, X. Z., Jia, Y. G., Xiong, J. G., and Peng, C. M. (2019). “Study on the Progressive Collapse Behavior of Fully Bolted RCS Beam-to-Column Connections.” Eng. Struct. 199: UNSP 109618.

Wang, H., Tan, K. H., and Yang, B. (2020). “Experimental Tests of Steel Frames with Different Beam-Column Connections under Falling Debris Impact.” J. Struct. Eng. 146 (1): 04019183.

Wang, J. J., Wang, W., and Qian, X. D. (2019). “Progressive Collapse Simulation of the Steel-Concrete Composite Floor System Considering Ductile Fracture of Steel.” Eng. Struct. 200: 109701.

Wang, W., Fang, C., Qin, X., Chen, Y. Y., and Li, L. (2016). “Performance of Practical Beam-to-SHS Column Connections against Progressive Collapse.” Eng. Struct. 106: 332-347.

Wang, W., Wang, J. J., Sun, X., and Bao, Y. H. (2017). “Slab Effect of Composite Subassemblies under a Column Removal Scenario.” J. Constr. Steel Res. 129: 141-155.

Yang, B., and Tan, K. H. (2012). “Component-Based Model of Bolted-Angle Connections Subjected to Catenary Action.” Proc. of the 10th Intl. Conf. on Advances in Steel Concrete Composite and Hybrid Structures. 654–61.

Yang, B., and Tan, K. H. (2013a). “Experimental Tests of Different Types of Bolted Steel Beam-Column Joints under a Central-Column-Removal Scenario.” Eng. Struct. 54: 112-130.

Yang, B., and Tan, K. H. (2013b). “Robustness of Bolted-Angle Connections against Progressive Collapse: Experimental Tests of Beam-Column Joints and Development of Component-Based Models.” J. Struct. Eng. 139 (9): 1498-1514.

Zhong, W. H., Tan, Z., Tian, L. M., Meng, B., Song, X. Y., and Zheng, Y. H. (2020). “Collapse Resistance of Composite Beam-Column Assemblies with Unequal Spans under an Internal Column-Removal Scenario.” Eng. Struct. 206: 110143.

## FIGURE CAPTIONS

**Fig. 1.** Location of the extracted frame in the prototype building (unit in mm): (a) plan view; (b) elevation view

**Fig. 2.** Dimensions of the specimen and locations of strain gauge and displacement transducers (unit in mm): (a) arrangements of strain gauges/rosettes and displacement transducers; (b) strain gauges positions on sections

**Fig. 3.** Geometric details of top-and-seat angle connection (unit in mm): (a) elevation view; (b) lateral view

**Fig. 4.** Test setups: (a) Schematic view of TSM-8; (b) Schematic view of TSP-8; (c) Schematic view of TSC-8; (d) Photograph of TSC-8

**Fig. 5.** Comparison of the load-displacement curves of specimens: TSC-8, TSP-8 and TSM-8

**Fig. 6.** Failure mode of TSC-8

**Fig. 7.** Failure mode of TSP-8

**Fig. 8.** Comparison of bending moment diagrams of the specimen: (a) excluding uniform load, (b) including uniform load

**Fig. 9.** Failure mode of TSM-8

**Fig. 10.** Comparison of the load-displacement curves of specimens: TSM-6, TSM-8 and TSM-10

**Fig. 11.** Failure mode of TSM-6

**Fig. 12.** Failure mode of TSM-10

**Fig. 13.** Horizontal reaction force-middle column displacement curves: (a) TSP-8; (b) TSM-8; (c) TSM-6; (d) TSM-10

**Fig. 14.** Horizontal movement of exterior joints: (a) TSP-8; (b) TSM-8; (c) TSM-6; (d) TSM-10

**Fig. 15.** Overall deflection profile of the beams in the first story: (a) TSC-8; (b) TSM-8

**Fig. 16.** Comparisons of the vertical load-displacement response from strain gauge and load cell: (a) TSC-8, TSM-8, TSP-8, TSM-6; (b) TSM-10

**Fig. 17.** Comparisons of horizontal reaction force-displacement response from strain gauge and load cell: (a) TSM-8, TSP-8, TSM-6; (b) TSM-10

**Fig. 18.** De-composition of the load resistance from different actions: (a) TSC-8; (b) TSP-8; (c) TSM-8; (d) TSM-6; (e) TSM-10 (Note: FA and CA represent flexural action and catenary action, respectively)

**Fig. 19.** De-composition of load resistance from 1st story and 2nd story: (a) TSC-8; (b) TSP-8; (c) TSM-8; (d) TSM-6; (e) TSM-10.

**Fig. 20.** Comparisons of the bending moment and axial force variation in 1st story and 2nd stories: (a) TSC-8; (b) TSP-8; (c) TSM-8; (d) TSM-6; (e) TSM-10.

**Fig. 21.** Moment-rotation behavior of connection.

**Fig. 22.** Simplification of the connection behavior: (a) idealized deformation pattern of connection; (b) equivalent springs of connection components

**Fig. 23.** Modelling of catenary action: (a) approximation of axial deformation; (b) structural representation.

**Fig. 24.** Tensile angle model

**Fig. 25.** Sketch of boundary condition assumption for analytical analysis

**Fig. 26.** Comparisons of test result and prediction model: (a) TSC-8; (b) TSP-8; (c) TSM-8; (d) TSM-6; (e) TSM-10

**Table 1-**Specimen properties

| Test ID | Column removal position | Angle section (mm) |
|---|---|---|
| TSC-8 | Corner | L70×8 |
| TSP -8 | Penultimate | L70×8 |
| TSM-8 | Middle | L70×8 |
| TSM-6 | Middle | L70×6 |
| TSM-10 | Middle | L70×10 |

**Table 2-**Material properties

| Items | Plate thickness (mm) | Yield strength (MPa) | Yield strain | Ultimate strength (MPa) | Ultimate strain | Elongation (%) |
|---|---|---|---|---|---|---|
| Beam flange | 8.0 | 310 | 0.0019 | 420 | 0.0240 | 12.0 |
| Beam web | 5.5 | 320 | 0.0021 | 430 | 0.0249 | 13.5 |
| Column flange | 10.0 | 300 | 0.0019 | 410 | 0.0267 | 14.0 |
| Column web | 7.0 | 295 | 0.0023 | 375 | 0.0242 | 13.0 |
| Angle 1 | 6.0 | 300 | 0.0018 | 425 | 0.0243 | 14.0 |
| Angle 2 | 8.0 | 310 | 0.0019 | 420 | 0.0276 | 12.0 |
| Angle 3 | 10.0 | 290 | 0.0018 | 430 | 0.0264 | 14.1 |

**Table 3-**Test results

| Test ID | $U_{YL}$ (mm) | $F_{YL}$ (kN) | $K_{YL}$ (kN/mm) | $U_{PL}$ (mm) | $F_{PL}$ (kN) |
|---|---|---|---|---|---|
| TSC-8 | 40 | 5.1 | 0.13 | 310 | 16.6 |
| TSP -8 | 20 | 11.0 | 0.55 | 564 | 39.8 |
| TSM-8 | 20 | 13.5 | 0.68 | 394 | 44.4 |
| TSM-6 | 19 | 9.3 | 0.49 | 289 | 34.0 |
| TSM-10 | 23 | 21.4 | 1.12 | 425 | 106.2 |

Note: $F_{YL}$ and $F_{PL}$ represent yield load and peak load, respectively; $U_{YL}$ and $U_{PL}$ represent displacements corresponding the yield load and peak load, respectively; $K_{YL}$ represents initial stiffness corresponding the yield load

**Table 4-**Comparisons between test results and analytical results

| Test ID | | $K_{YL}$ (kN/mm) | Discrepancy | $F_{YL}$ (kN) | Discrepancy | $U_{FF}$ (mm) | Discrepancy | $F_{FF}$ (kN) | Discrepancy |
|---|---|---|---|---|---|---|---|---|---|
| TSC-8 | Test data | 0.13 | 1.5% | 5.1 | 2.1% | 310 | 14.9% | 16.6 | 5.8% |
| | Analytical results | 0.13 | | 5.2 | | 356 | | 17.6 | |
| TSP-8 | Test data | 0.55 | 22.3% | 11.0 | 32.1% | 295 | 20.5% | 36.7 | 0.2% |
| | Analytical results | 0.67 | | 14.6 | | 356 | | 36.7 | |
| TSM-8 | Test data | 0.68 | 29.2% | 13.5 | -3.7% | 289 | -5.1% | 41.3 | -2.6% |
| | Analytical results | 0.87 | | 13.0 | | 274 | | 40.2 | |
| TSM-6 | Test data | 0.49 | 52.9% | 9.3 | -7.4% | 289 | 1.5% | 34.0 | 5.6% |
| | Analytical results | 0.75 | | 8.6 | | 293 | | 35.9 | |
| TSM-10 | Test data | 1.12 | 2.0% | 21.4 | 49.5% | 425 | -8.8% | 106.2 | -1.7% |
| | Analytical results | 1.14 | | 32.0 | | 388 | | 104.4 | |

Note: $U_{FF}$ and $F_{FF}$ represent the vertical displacement and vertical load corresponding the first fracture

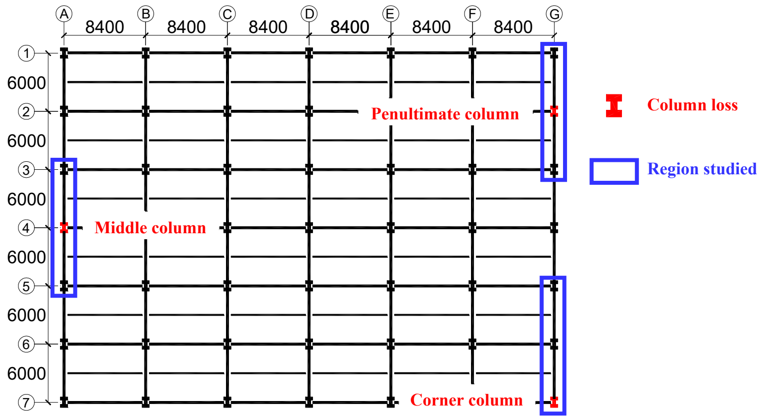
A
B
C
D
E
F
G
8400
8400
8400
8400
8400
8400
1
2
3
4
5
6
7
6000
6000
6000
6000
6000
6000
Penultimate column
Middle column
Corner column
Column loss
Region studied

(a)

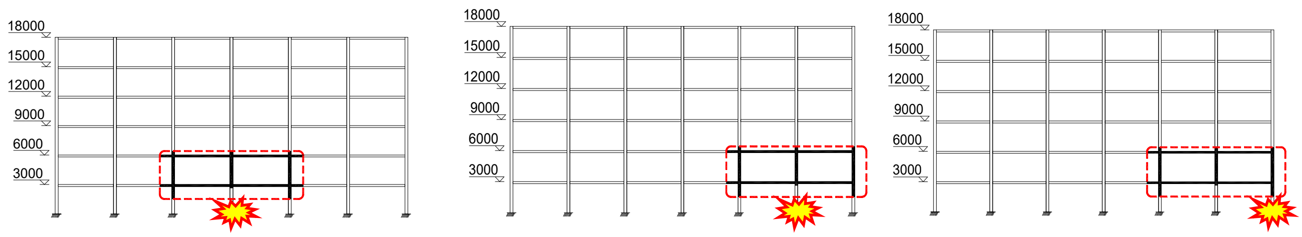
18000
15000
12000
9000
6000
3000

(b)

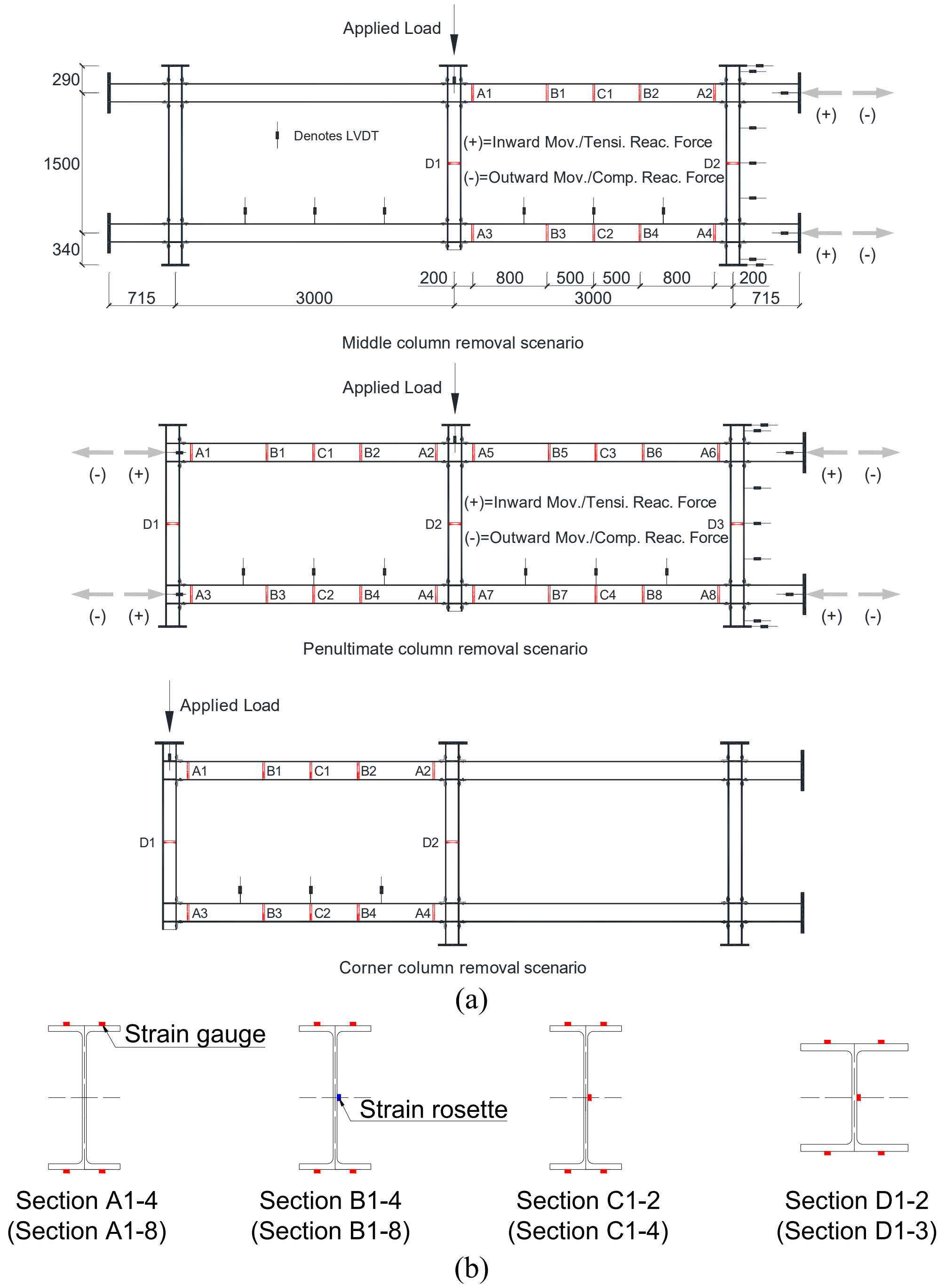
Applied Load
290
1500
340
Denotes LVDT
A1 B1 C1 B2 A2
A3 B3 C2 B4 A4
D1
D2
(+)=Inward Mov./Tensi. Reac. Force
(-)=Outward Mov./Comp. Reac. Force
(+) (-)
200 800 500 500 800 200
715 3000 3000 715
Middle column removal scenario
Applied Load
A1 B1 C1 B2 A2 A5 B5 C3 B6 A6
A3 B3 C2 B4 A4 A7 B7 C4 B8 A8
D1
D2
D3
(+)=Inward Mov./Tensi. Reac. Force
(-)=Outward Mov./Comp. Reac. Force
(-) (+)
Penultimate column removal scenario
Applied Load
A1 B1 C1 B2 A2
A3 B3 C2 B4 A4
D1
D2
Corner column removal scenario
(a)
Strain gauge
Strain rosette
Section A1-4
(Section A1-8)
Section B1-4
(Section B1-8)
Section C1-2
(Section C1-4)
Section D1-2
(Section D1-3)
(b)

Figure 3



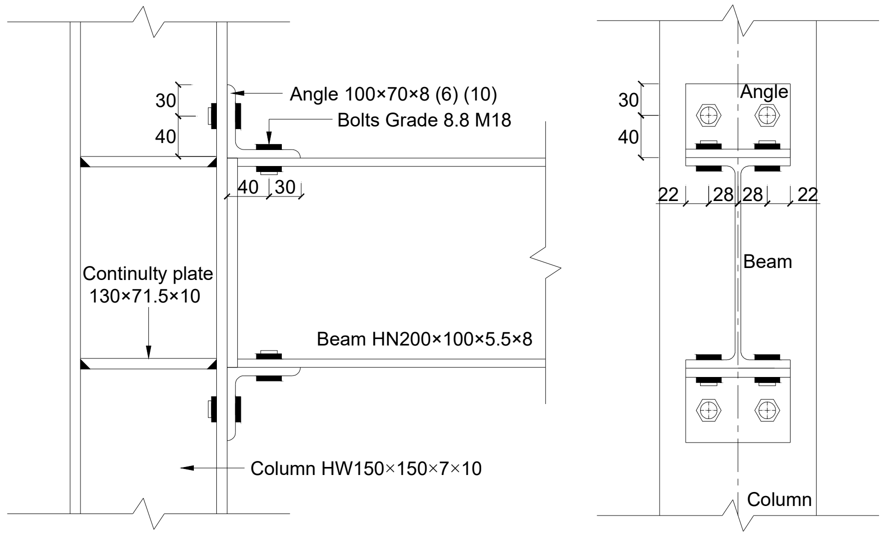
Angle 100×70×8 (6) (10)
Bolts Grade 8.8 M18
30
40
40
30
Continulty plate
130×71.5×10
Beam HN200×100×5.5×8
Column HW150×150×7×10
30
40
Angle
22
28
28
22
Beam
Column

(a) (b)

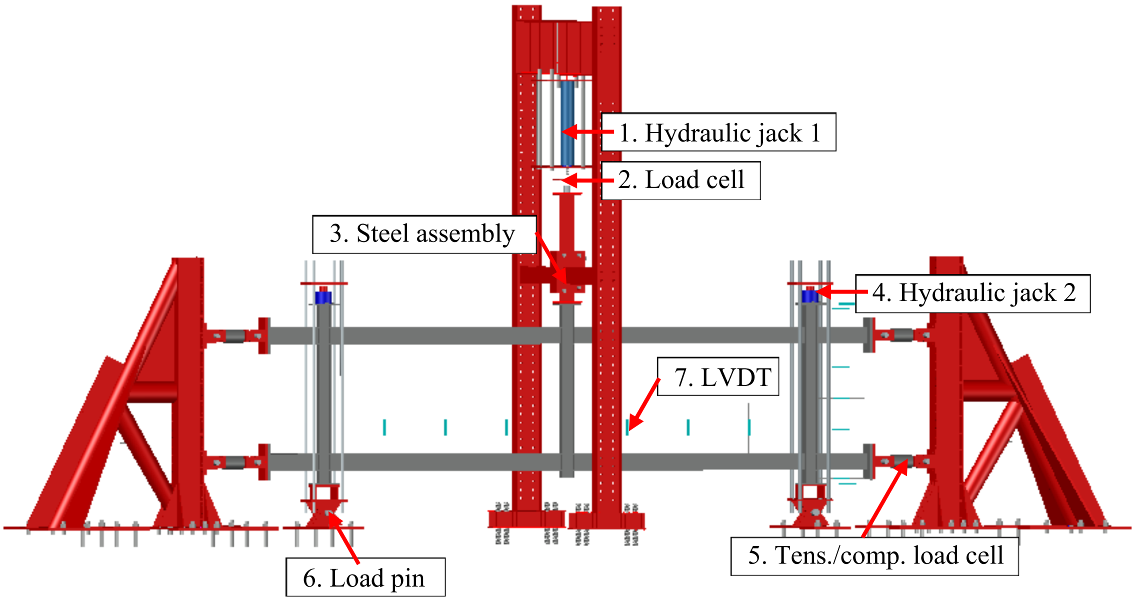
1. Hydraulic jack 1
2. Load cell
3. Steel assembly
4. Hydraulic jack 2
7. LVDT
5. Tens./comp. load cell
6. Load pin

(a)

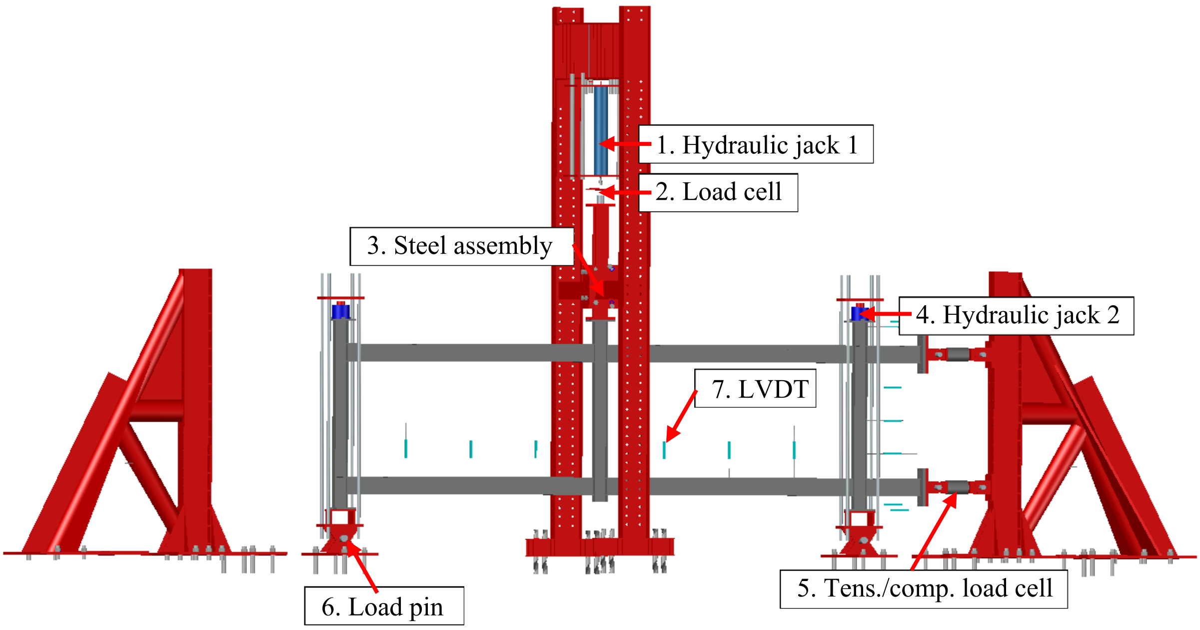
1. Hydraulic jack 1
2. Load cell
3. Steel assembly
4. Hydraulic jack 2
7. LVDT
5. Tens./comp. load cell
6. Load pin

(b)

Figure 4-2



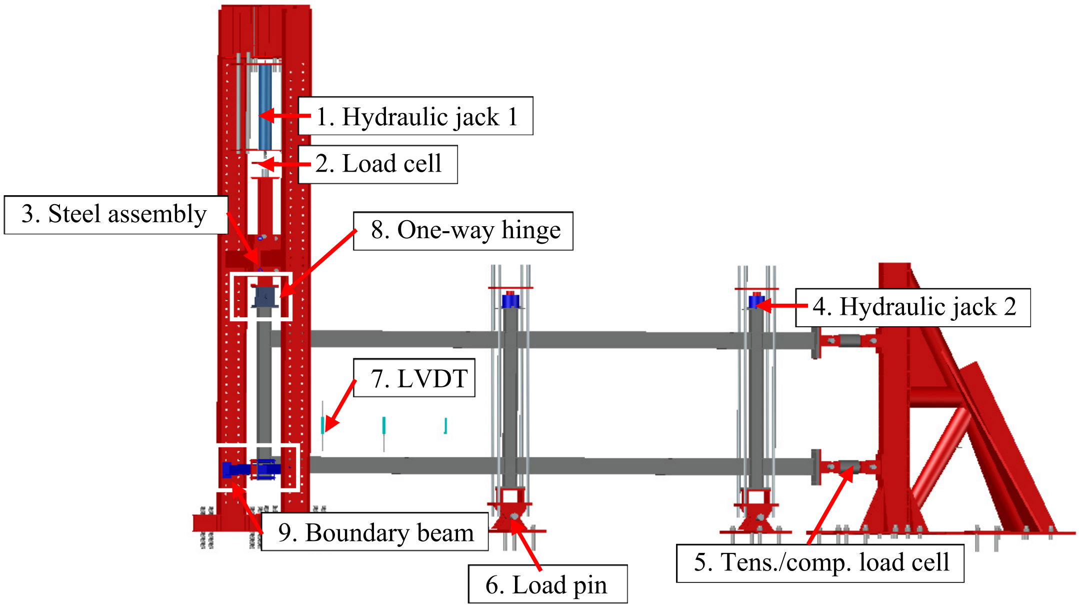
1. Hydraulic jack 1
2. Load cell
3. Steel assembly
8. One-way hinge
4. Hydraulic jack 2
7. LVDT
9. Boundary beam
6. Load pin
5. Tens./comp. load cell

(c)

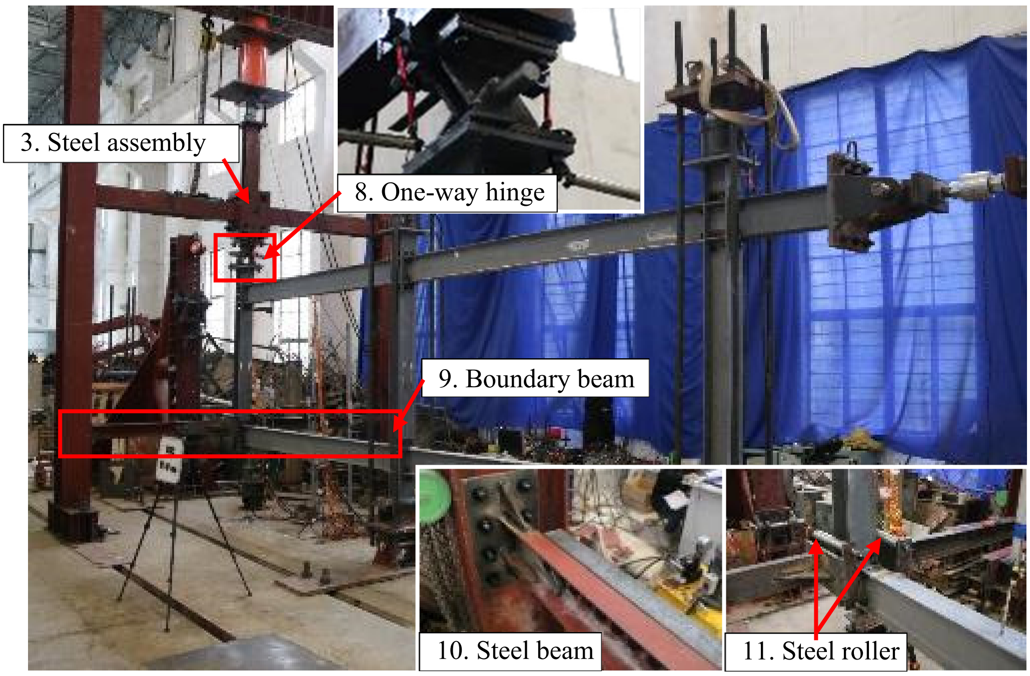
3. Steel assembly
8. One-way hinge
9. Boundary beam
10. Steel beam
11. Steel roller

(d)

Figure 5



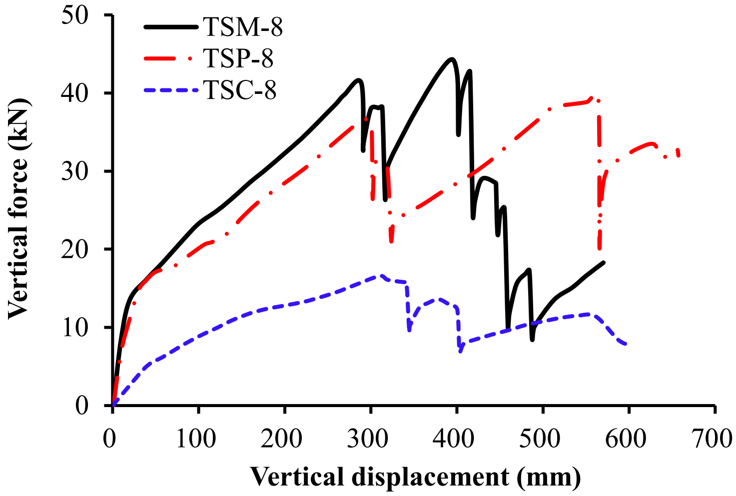

TSM-8
TSP-8
TSC-8
Vertical force (kN)
0
10
20
30
40
50
0
100
200
300
400
500
600
700
Vertical displacement (mm)

Figure 6



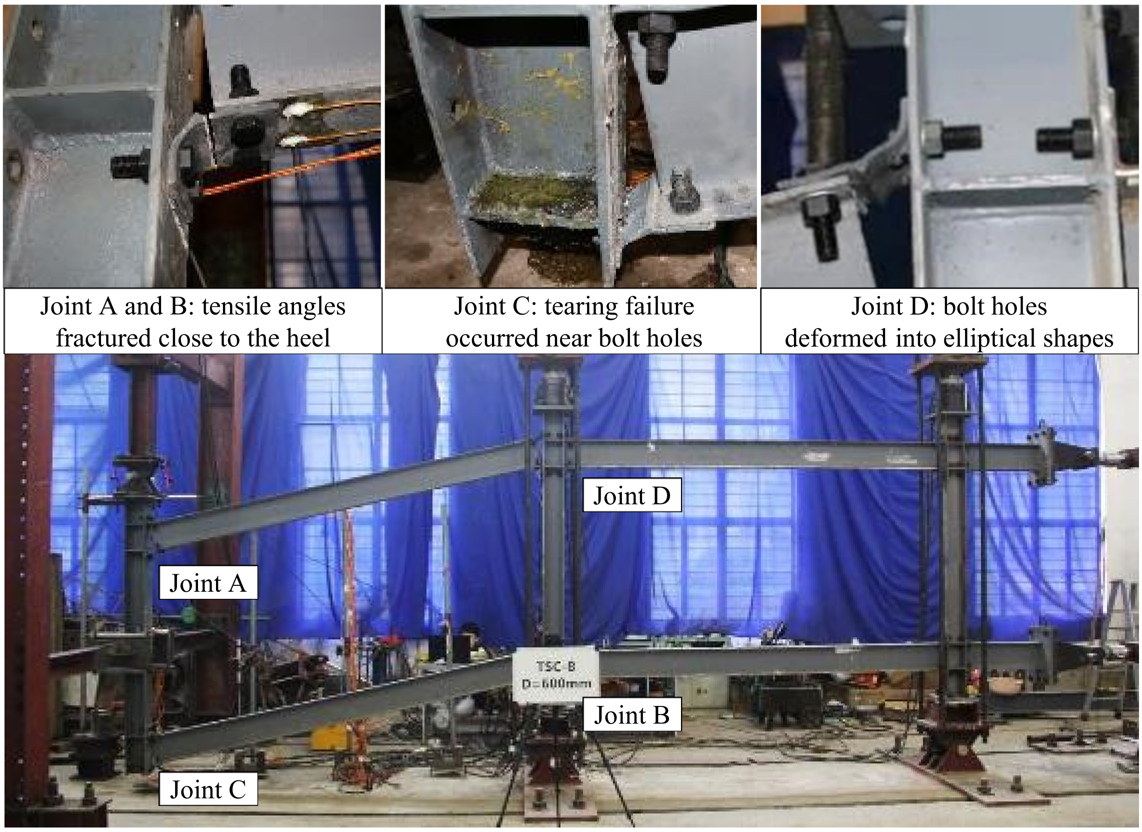
Joint A and B: tensile angles fractured close to the heel
Joint C: tearing failure occurred near bolt holes
Joint D: bolt holes deformed into elliptical shapes
Joint D
Joint A
Joint B
Joint C

Figure 7



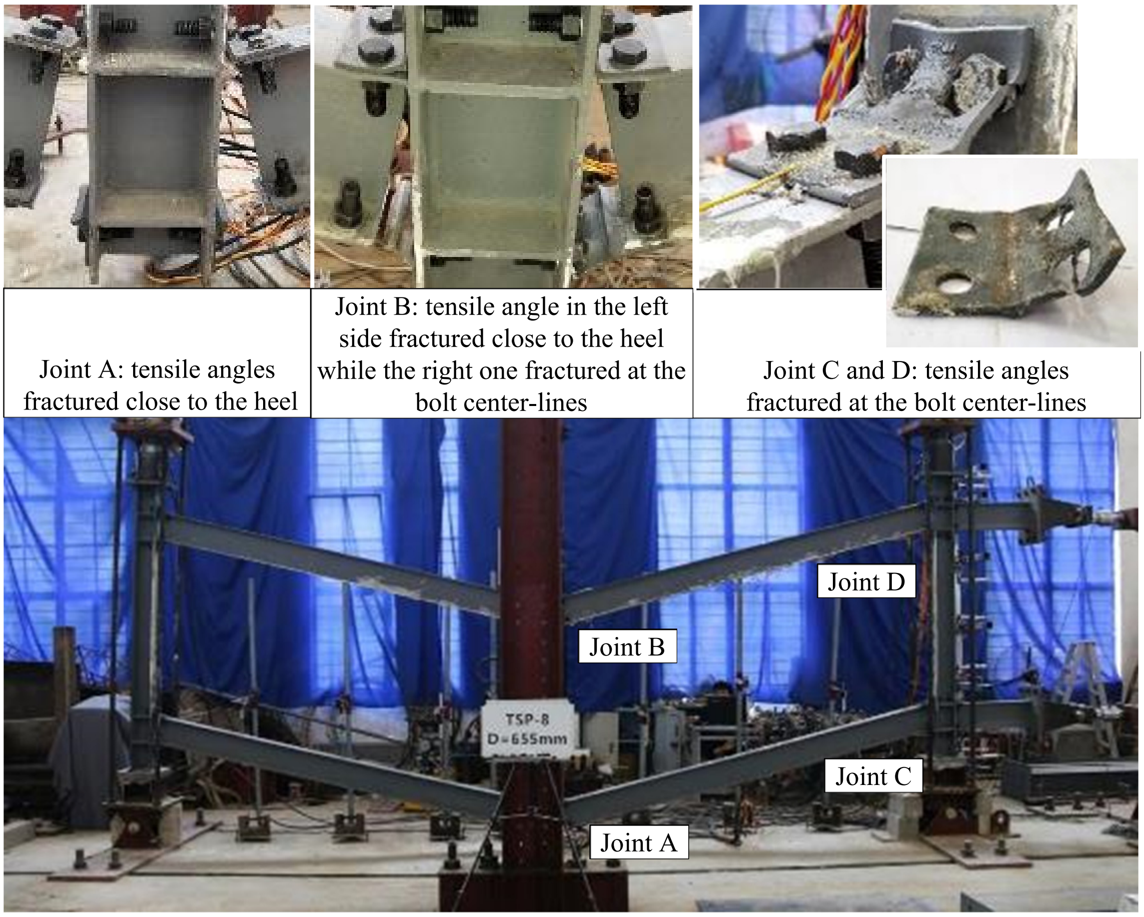
Joint A: tensile angles fractured close to the heel
Joint B: tensile angle in the left side fractured close to the heel while the right one fractured at the bolt center-lines
Joint C and D: tensile angles fractured at the bolt center-lines
Joint D
Joint B
TSP-8
D=655mm
Joint C
Joint A

Figure 8



1

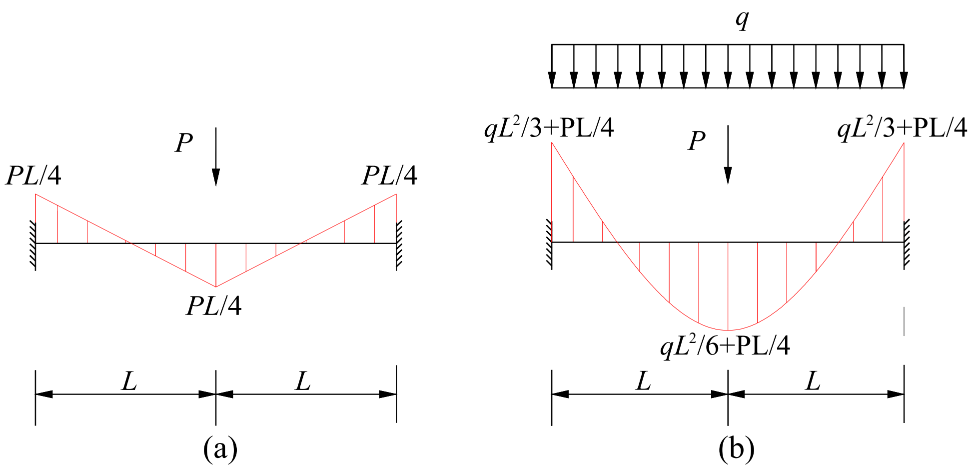

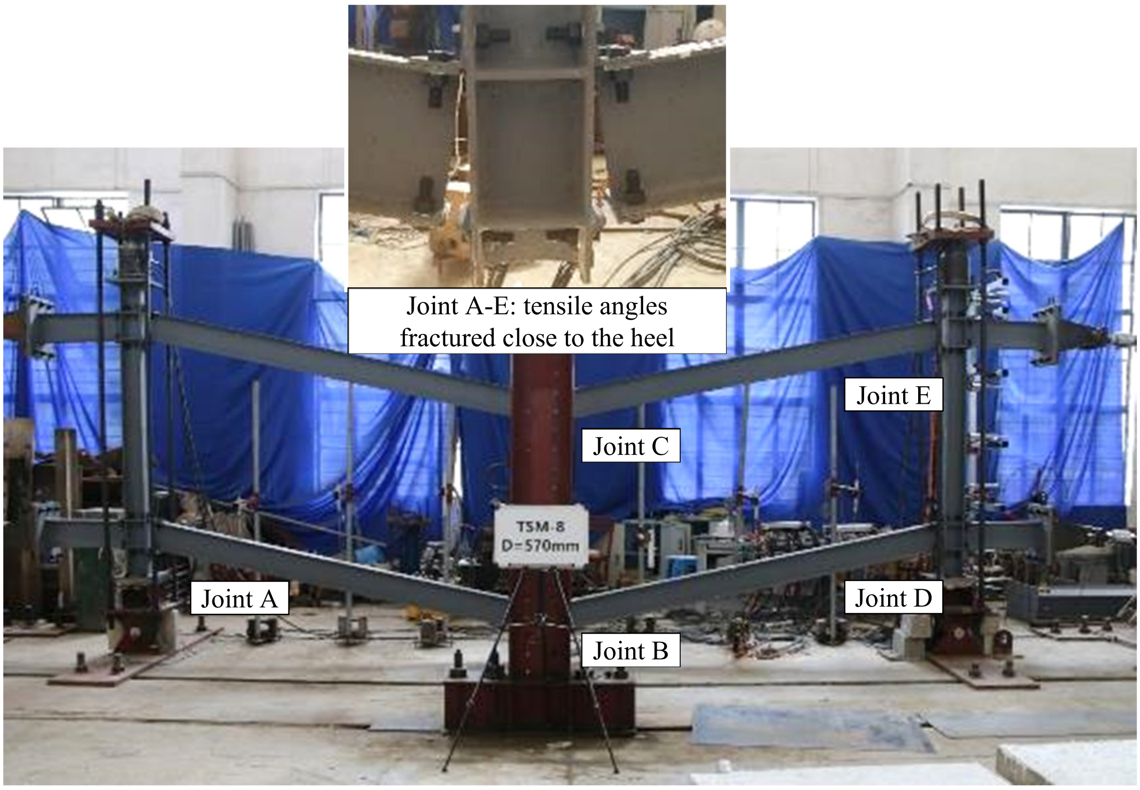
Joint A-E: tensile angles
fractured close to the heel
Joint E
Joint C
TSM-8
D=570mm
Joint A
Joint D
Joint B

Figure 10



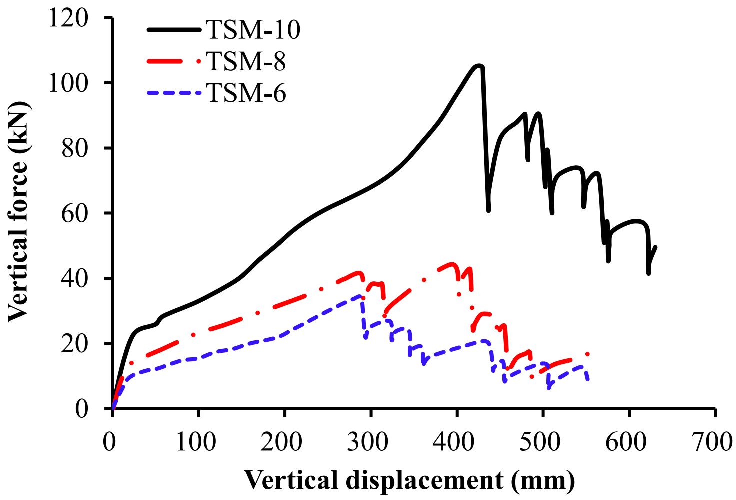

Vertical force (kN)
120
100
80
60
40
20
0
TSM-10
TSM-8
TSM-6
0
100
200
300
400
500
600
700
Vertical displacement (mm)

Figure 11



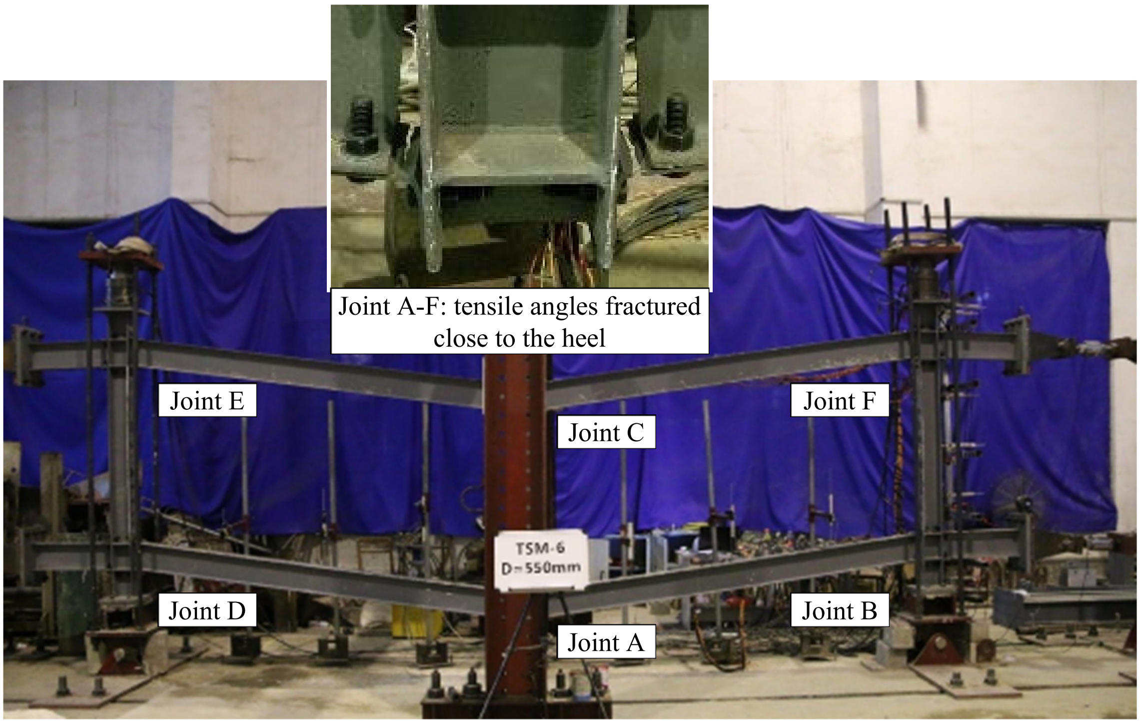
Joint A-F: tensile angles fractured close to the heel
Joint E
Joint F
Joint C
TSM-6
D=550mm
Joint D
Joint B
Joint A

Figure 12



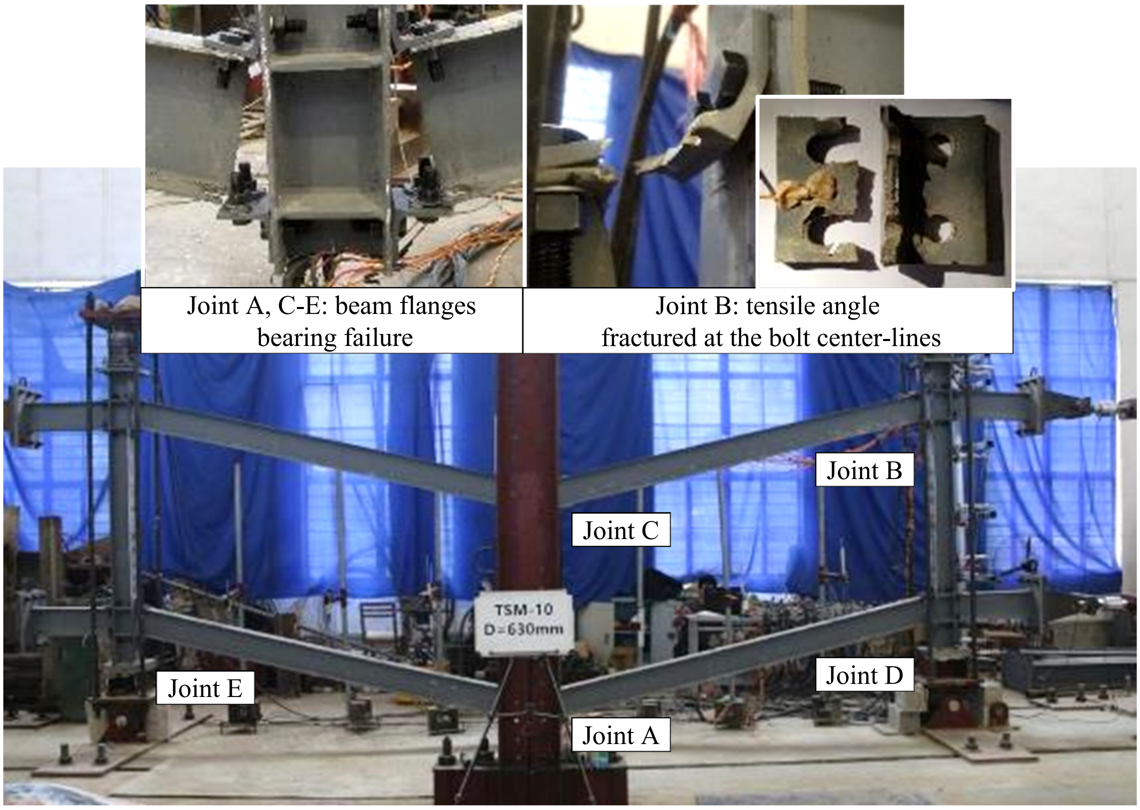
Joint A, C-E: beam flanges
bearing failure
Joint B: tensile angle
fractured at the bolt center-lines
Joint B
Joint C
TSM-10
D=630mm
Joint E
Joint D
Joint A

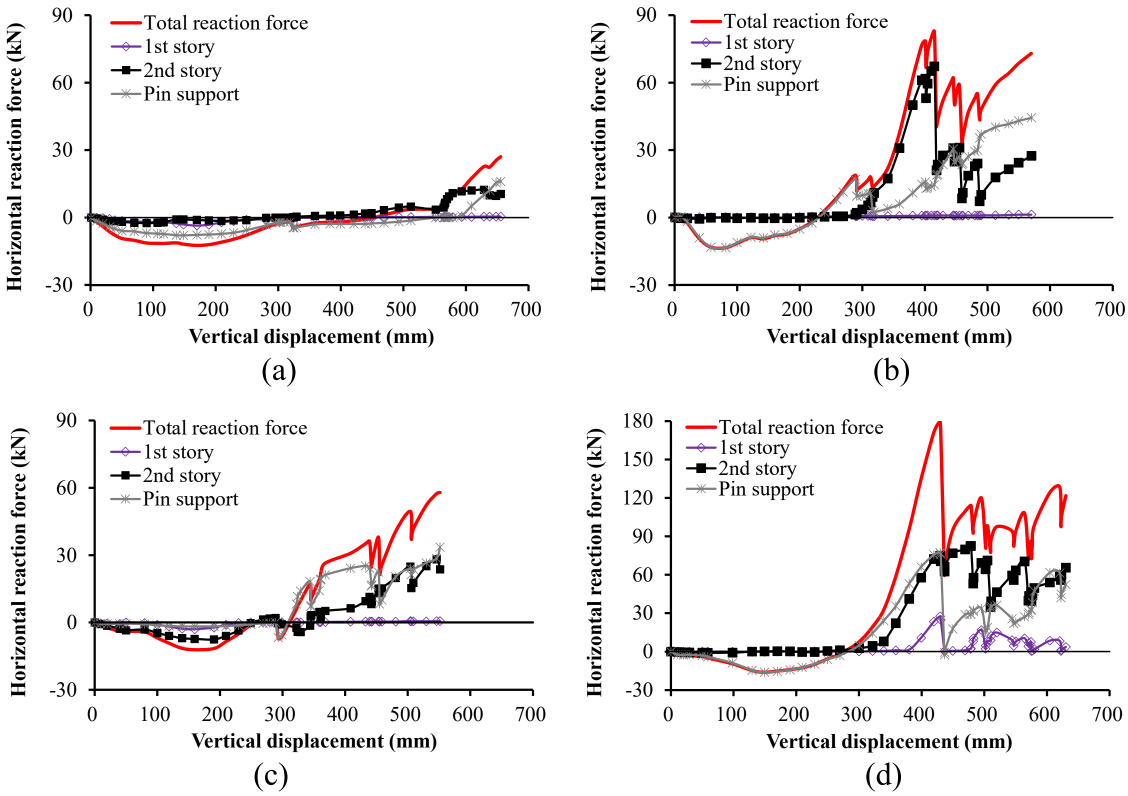
Total reaction force
1st story
2nd story
Pin support
Horizontal reaction force (kN)
Vertical displacement (mm)
(a)
(b)
(c)
(d)

 

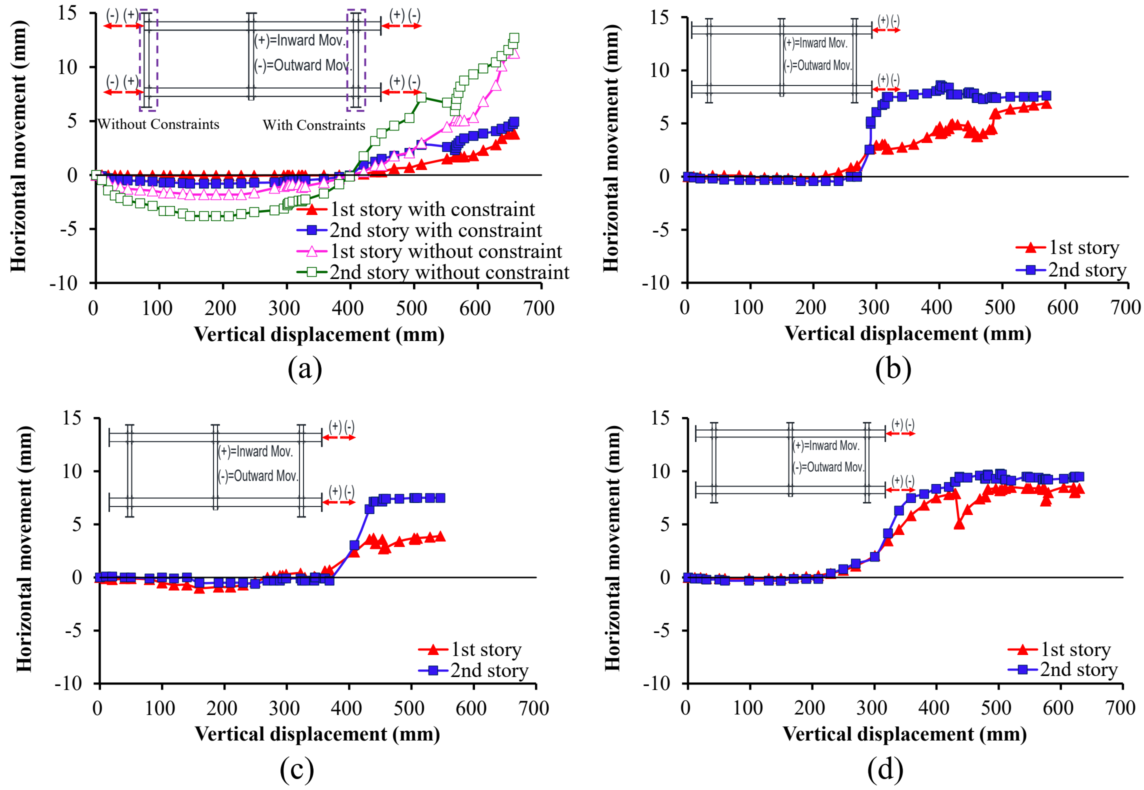
(+)=Inward Mov.
(-)=Outward Mov.
Without Constraints
With Constraints
1st story with constraint
2nd story with constraint
1st story without constraint
2nd story without constraint
1st story
2nd story
Horizontal movement (mm)
Vertical displacement (mm)
(a)
(b)
(c)
(d)

Figure 15



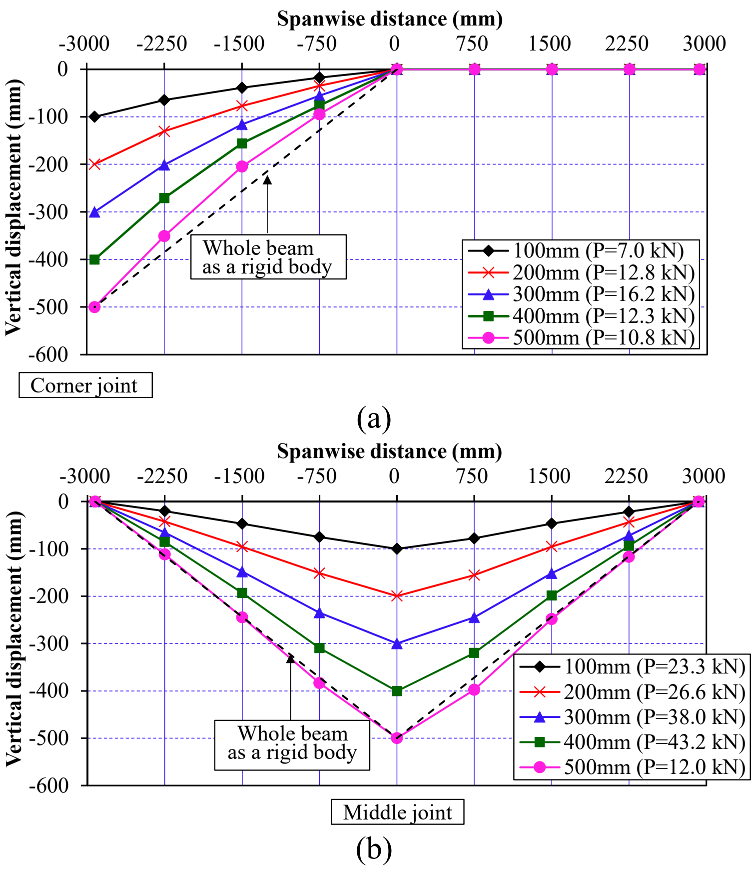

Spanwise distance (mm)
-3000
-2250
-1500
-750
0
750
1500
2250
3000
Vertical displacement (mm)
0
-100
-200
-300
-400
-500
-600
Whole beam
as a rigid body
100mm (P=7.0 kN)
200mm (P=12.8 kN)
300mm (P=16.2 kN)
400mm (P=12.3 kN)
500mm (P=10.8 kN)
Corner joint
(a)
Spanwise distance (mm)
Vertical displacement (mm)
100mm (P=23.3 kN)
200mm (P=26.6 kN)
300mm (P=38.0 kN)
400mm (P=43.2 kN)
500mm (P=12.0 kN)
Whole beam
as a rigid body
Middle joint
(b)

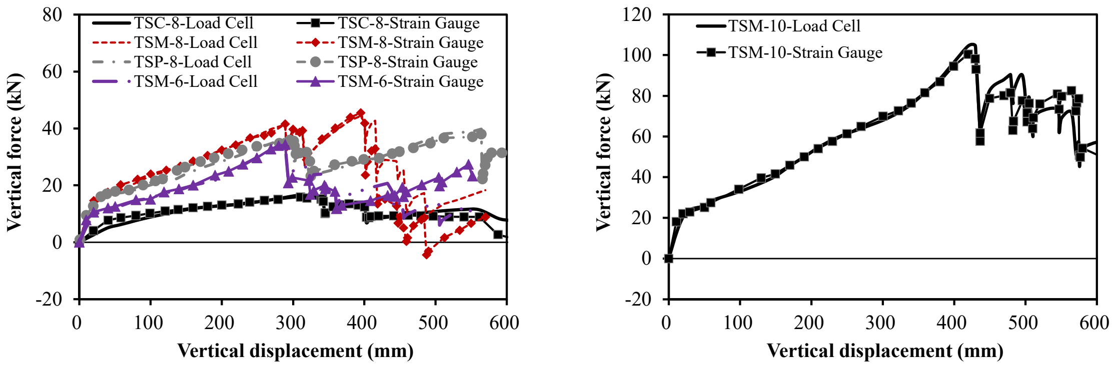
TSC-8-Load Cell
TSC-8-Strain Gauge
TSM-8-Load Cell
TSM-8-Strain Gauge
TSP-8-Load Cell
TSP-8-Strain Gauge
TSM-6-Load Cell
TSM-6-Strain Gauge
Vertical force (kN)
Vertical displacement (mm)
TSM-10-Load Cell
TSM-10-Strain Gauge
Vertical force (kN)
Vertical displacement (mm)

(a) (b)

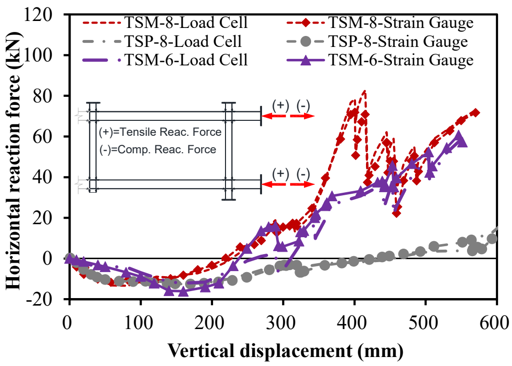
TSM-8-Load Cell
TSM-8-Strain Gauge
TSP-8-Load Cell
TSP-8-Strain Gauge
TSM-6-Load Cell
TSM-6-Strain Gauge
(+)=Tensile Reac. Force
(-)=Comp. Reac. Force
(+) (-)
(+) (-)
Horizontal reaction force (kN)
Vertical displacement (mm)
120
100
80
60
40
20
0
-20
0
100
200
300
400
500
600

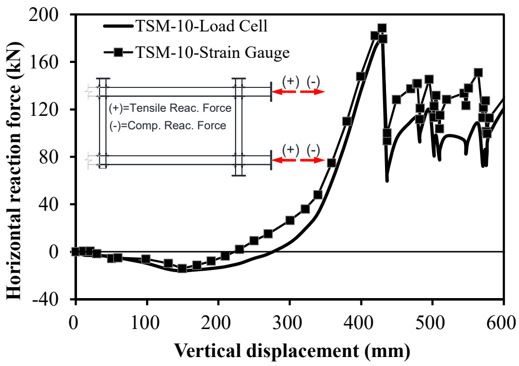
TSM-10-Load Cell
TSM-10-Strain Gauge
(+)=Tensile Reac. Force
(-)=Comp. Reac. Force
(+) (-)
(+) (-)
Horizontal reaction force (kN)
Vertical displacement (mm)
200
160
120
80
40
0
-40
0
100
200
300
400
500
600

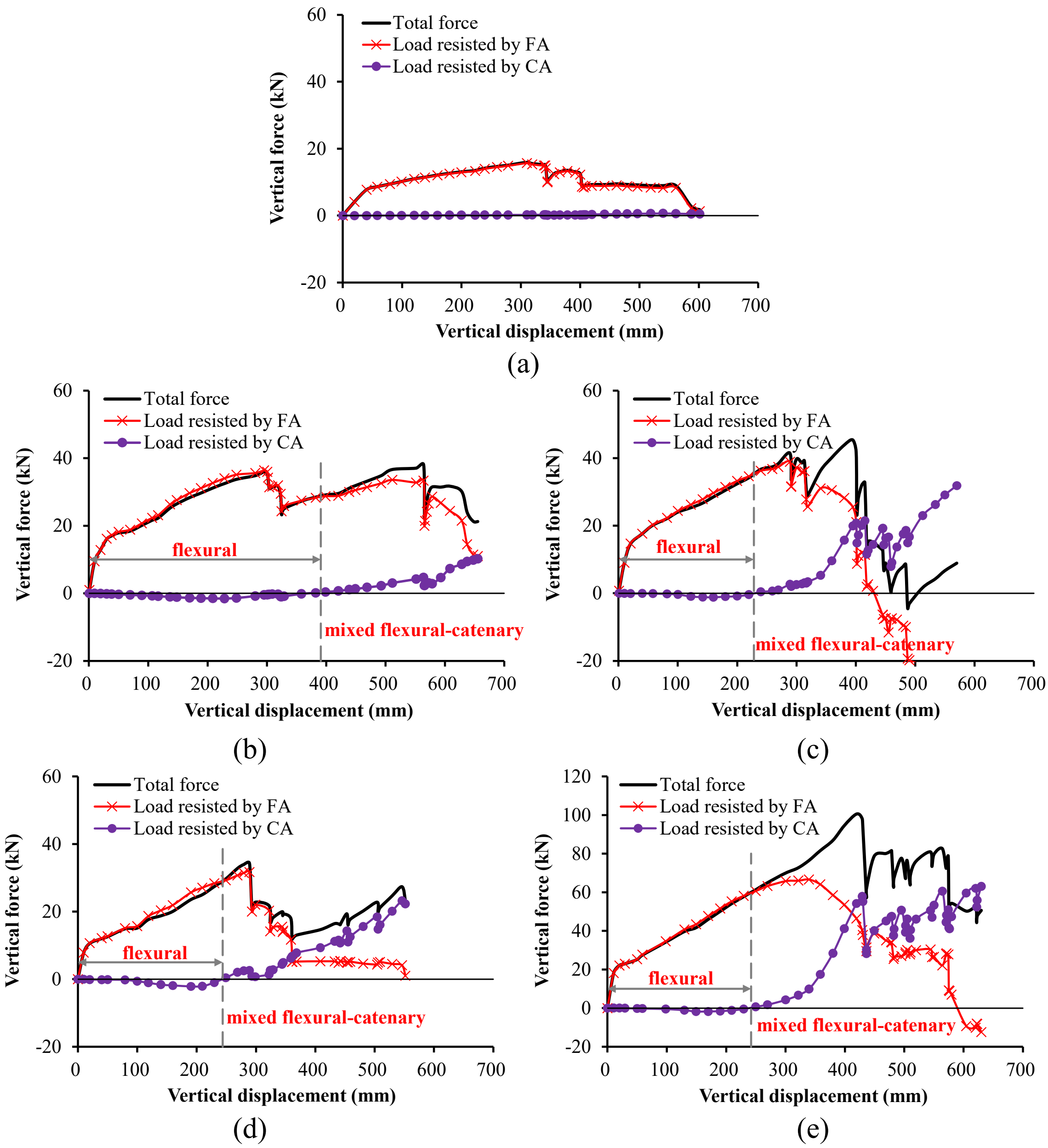
Total force
Load resisted by FA
Load resisted by CA
Vertical force (kN)
Vertical displacement (mm)
flexural
mixed flexural-catenary
(a)
(b)
(c)
(d)
(e)

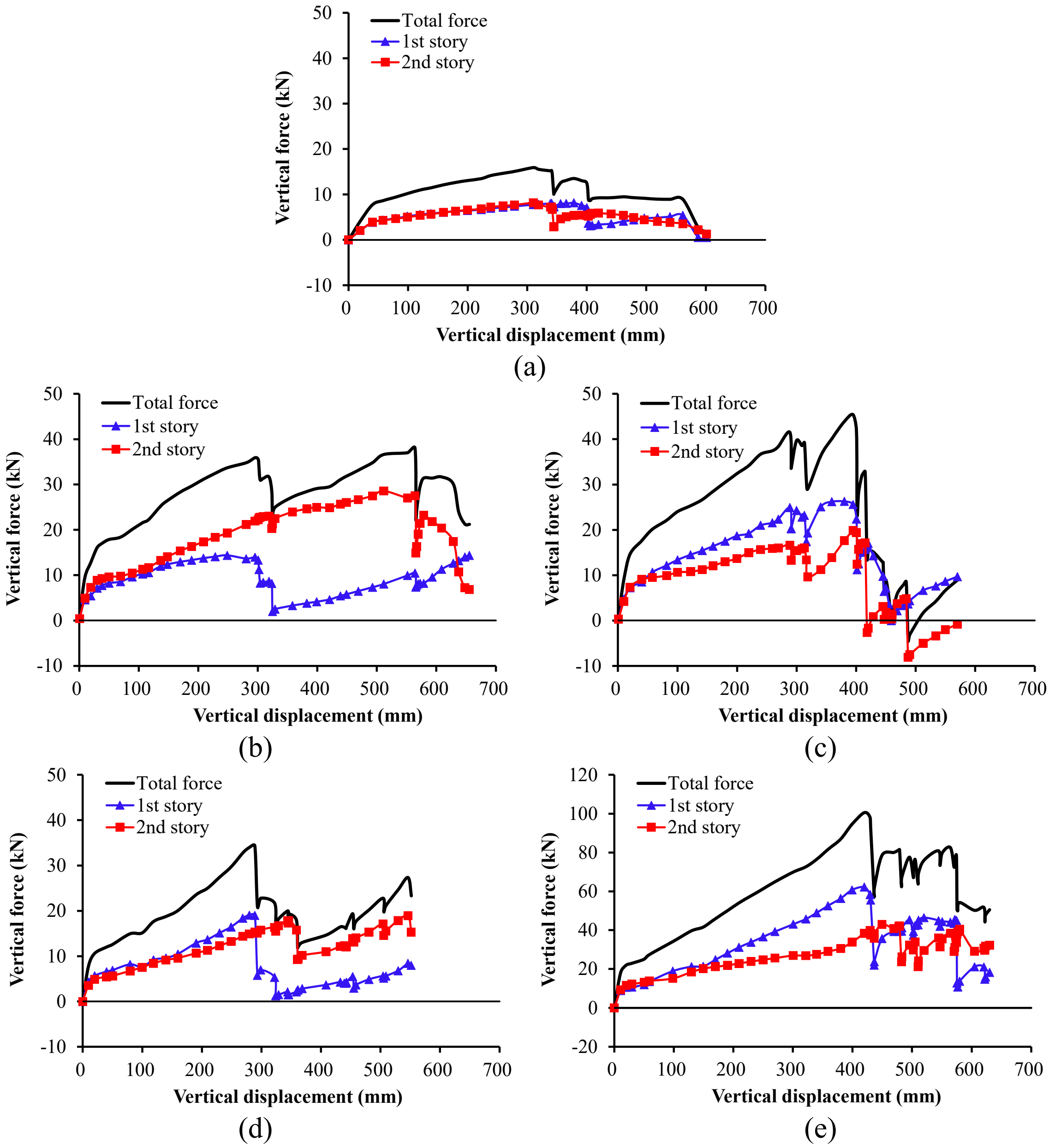
Total force
1st story
2nd story
Vertical force (kN)
Vertical displacement (mm)
(a)
(b)
(c)
(d)
(e)

Figure 20

Click here to access/download;Figure;Fig. B20.pdf

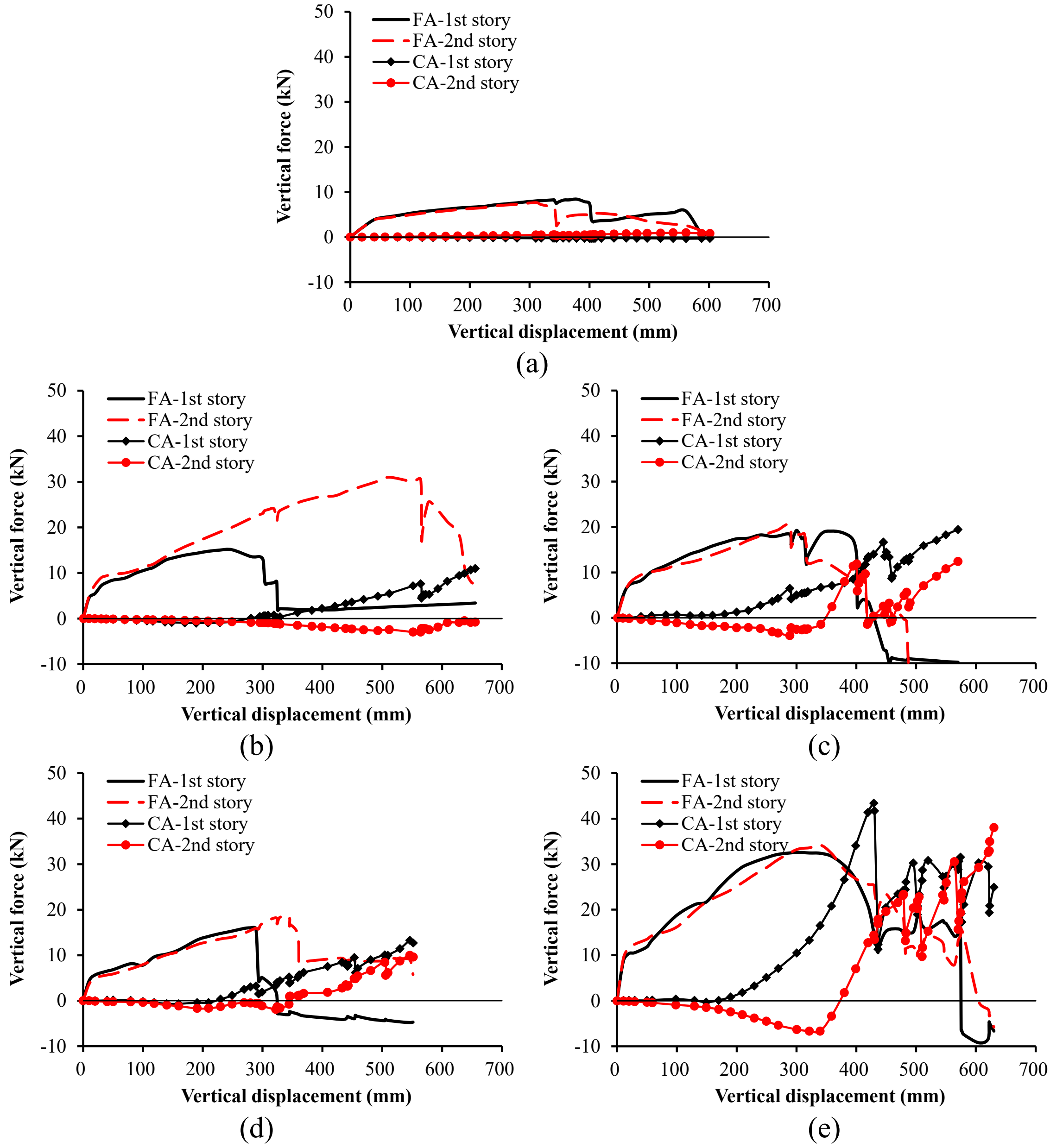

Figure 21



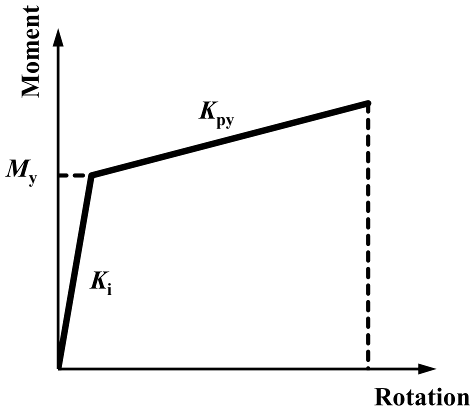

 

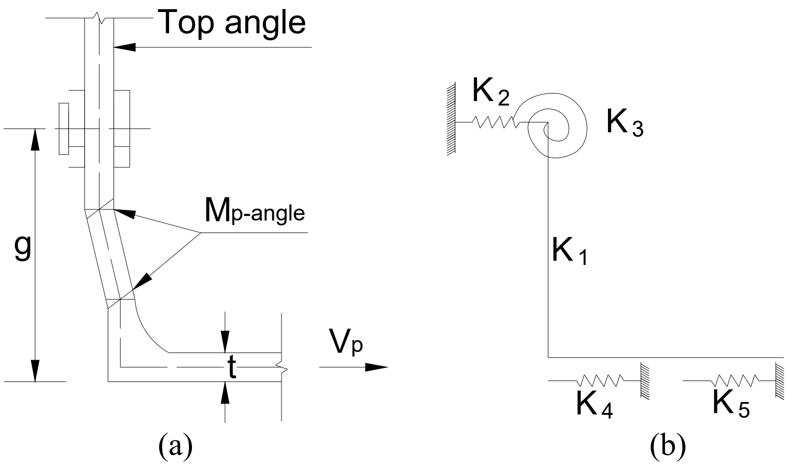

Top angle
$M_{p\text{-angle}}$
g
t
$V_p$
(a)
$K_2$
$K_3$
$K_1$
$K_4$
$K_5$
(b)

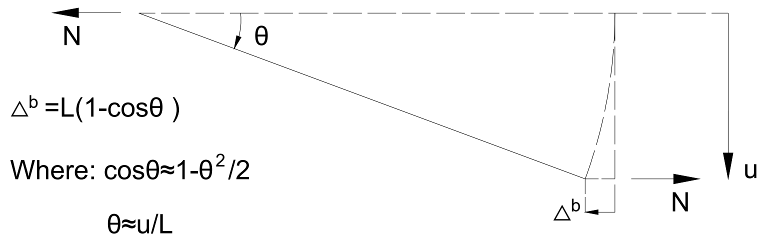


(a)

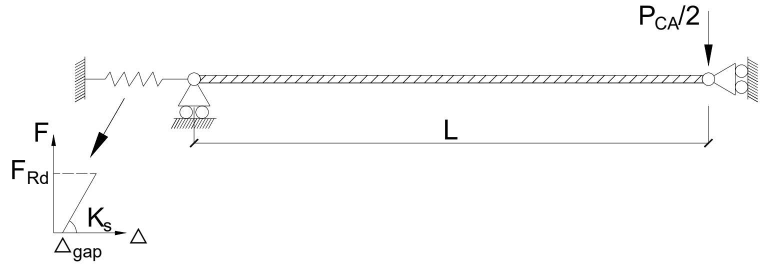


(b)

 

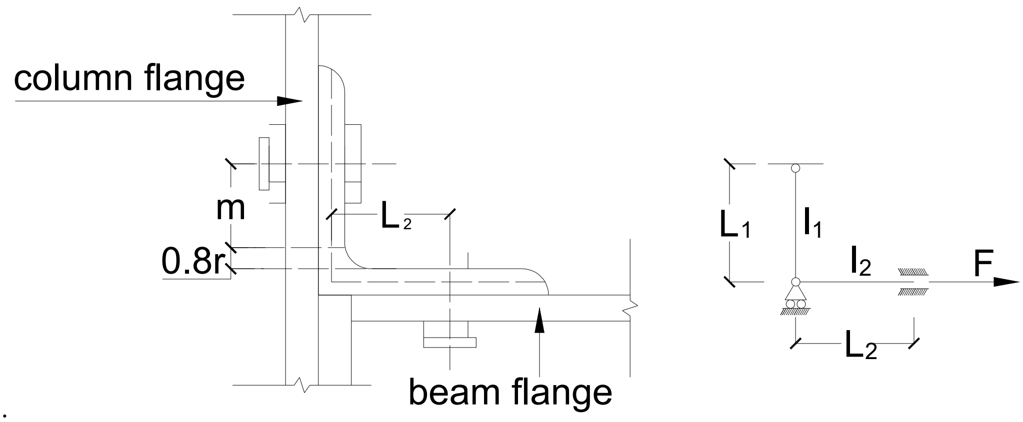
column flange
m
0.8r
L2
beam flange
L1
l1
l2
F
L2

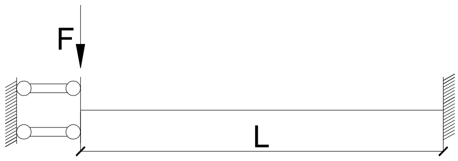


(a) full constraints

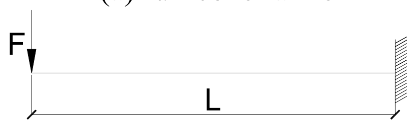


(b) free constraints

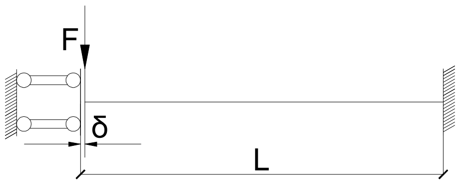


(c) partial constraints

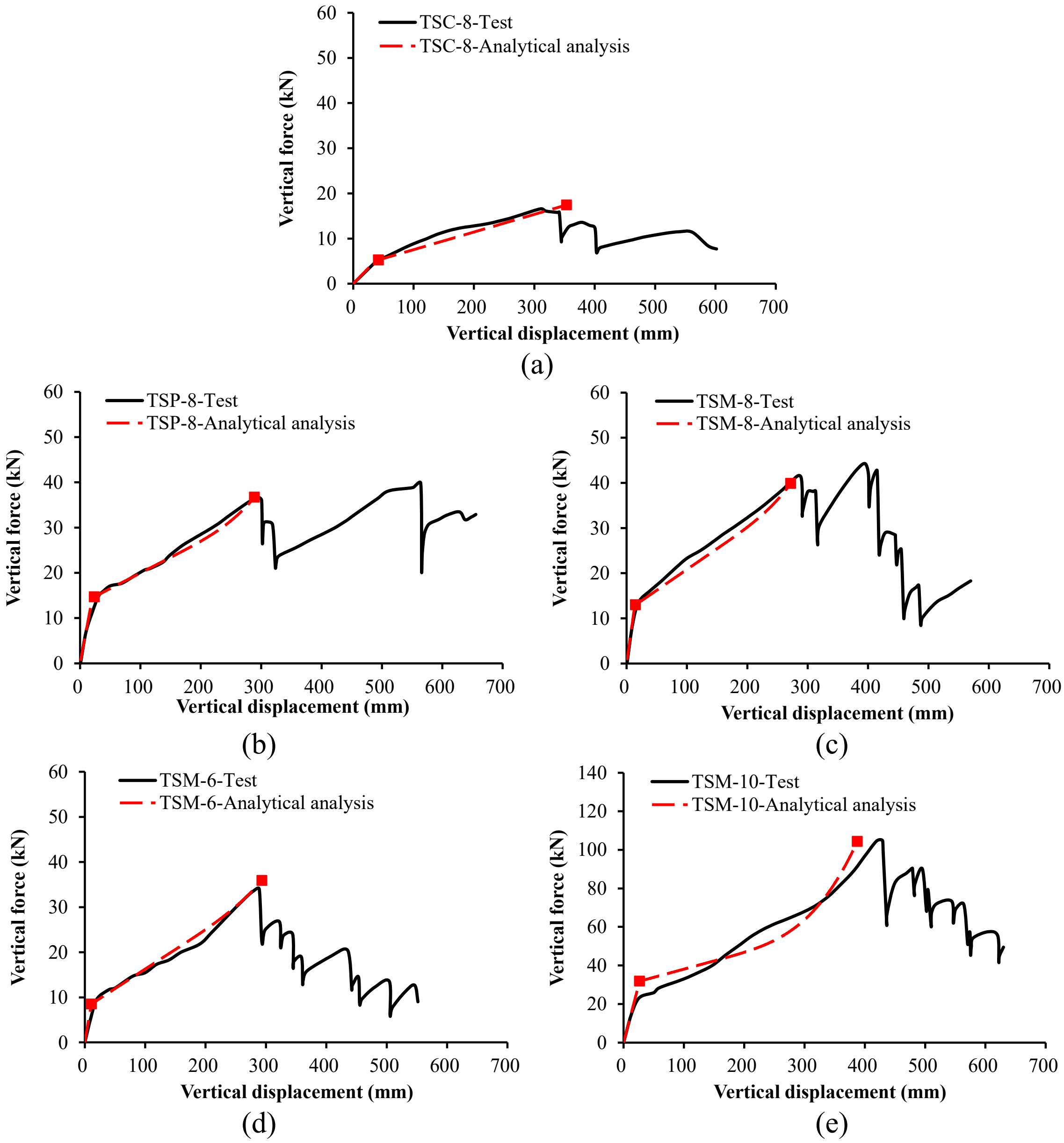
TSC-8-Test
TSC-8-Analytical analysis
Vertical force (kN)
Vertical displacement (mm)
0
10
20
30
40
50
60
0
100
200
300
400
500
600
700
(a)
TSP-8-Test
TSP-8-Analytical analysis
Vertical force (kN)
Vertical displacement (mm)
(b)
TSM-8-Test
TSM-8-Analytical analysis
Vertical force (kN)
Vertical displacement (mm)
(c)
TSM-6-Test
TSM-6-Analytical analysis
Vertical force (kN)
Vertical displacement (mm)
(d)
TSM-10-Test
TSM-10-Analytical analysis
Vertical force (kN)
Vertical displacement (mm)
80
100
120
140
(e)